NASA CONTRACTOR REPORT

NASA CR-2864

NONPLANAR WING LOAD-LINE AND SLENDER WING THEORY

John DeYoung

Prepared by
VOUGHT CORPORATION HAMPTON TECHNICAL CENTER
Hampton, Va. 23666
for Langley Research Center

NATIONAL AERONAUTICS AND SPACE ADMINISTRATION • WASHINGTON D. C. • AUGUST 1977

1. Report No.	2. Government Accession No.	3. Recipient's Catalog No.
NASA CR-2864		

4. Title and Subtitle	5. Report Date
NONPLANAR WING LOAD-LINE AND SLENDER WING THEORY	August 1977
	6. Performing Organization Code

7. Author(s)	8. Performing Organization Report No.
John DeYoung	

9. Performing Organization Name and Address	10. Work Unit No.
Vought Corporation Hampton Technical Center 3221 North Armistead Avenue Hampton, Virginia 23666	791-40-08-01
	11. Contract or Grant No. NAS1-13500

12. Sponsoring Agency Name and Address	13. Type of Report and Period Covered
National Aeronautics & Space Administration Washington, D. C.	Contractor Report
	14. Sponsoring Agency Code

15. Supplementary Notes

Langley technical monitor: Harry H. Heyson
Topical report.

16. Abstract Nonplanar load line, slender wing, elliptic wing, and infinite aspect ratio limit, loading theories are developed. These are quasi two-dimensional theories but satisfy wing boundary conditions at all points along the nonplanar spanwise extent of the wing. These methods are applicable for generalized configurations such as the laterally nonplanar wing, multiple nonplanar wings, or wing with multiple winglets of arbitrary shape. Two-dimensional theory infers simplicity which is practical when analyzing complicated configurations. The lateral spanwise distribution of angle of attack can be that due to winglet or control surface deflection, wing twist, or induced angles due to multiwings, multiwinglets, ground, walls, jet or fuselage. In a quasi two-dimensional theory the induced angles due to these extra conditions are likewise determined for two-dimensional flow. Equations are developed for the normal to surface induced velocity due to a nonplanar trailing vorticity distribution. Application examples are made using these methods.

17. Key Words (Suggested by Author(s))	18. Distribution Statement
Nonplanar Wing Theory Nonplanar Slender Wing Theory Winglet Theory Spanwise Loading Wing Aerodynamics	Unclassified - Unlimited Subject Category 02

19. Security Classif. (of this report)	20. Security Classif. (of this page)	21. No. of Pages	22. Price*
Unclassified	Unclassified	76	$5.00

* For sale by the National Technical Information Service, Springfield, Virginia 22161

TABLE OF CONTENTS

NONPLANAR WING LOAD-LINE AND SLENDER WING THEORY

By John DeYoung
Vought Corporation Hampton Technical Center

SUMMARY

Nonplanar load line, slender wing, elliptic wing, and infinite aspect ratio limit, loading theories are developed. These are quasi two-dimensional theories but satisfy wing boundary conditions at all points along the nonplanar spanwise extent of the wing. These methods are applicable for generalized configurations such as the laterally nonplanar wing, multiple nonplanar wings, or wing with multiple winglets of arbitrary shape. Two-dimensional theory infers simplicity which is practical when analyzing complicated configurations. The lateral spanwise distribution of angle of attack can be that due to winglet or control surface deflection, wing twist, or induced angles due to multiwings, multiwinglets, ground, walls, jet, or fuselage. In a quasi two-dimensional theory the induced angles due to these extra conditions are likewise determined for two-dimensional flow. Equations are developed for the normal to surface induced velocity due to a nonplanar trailing vorticity distribution. Example application of these methods are made for a rectangular wing with wingtip winglets. Compared with a planar wing, induced drag is reduced 5, 13, 66 percent for aspect ratios of 0, 10.9, and infinity. The same results apply to a 30° swept wing with 0.29 taper ratio and smaller aspect ratio.

INTRODUCTION

Theories for multiplane systems and wing endplate theories span the history of aerodynamic theory. Early analytical solutions are detailed in reference 1. Theoretical development tended to follow the needs of aircraft design. In the beginning aircraft were multiplanes including biplanes and triplanes. Two-dimensional airfoil tunnel tests in Europe were

traditionally models of sections with endplates. These required corrections from wing with endplates to two-dimensional section data. In reference 2 by solutions in the Trefftz plane the induced drags are determined of many wingtip configurations. These include vertical plates at various span stations, circular bodies, and array of fins. Some of these wingtip configurations were computed with electromagnetic analogy methods. Winglet concepts advanced by Whitcomb are presented in reference 3. These are uniquely designed angled wingtip fins for minimizing induced drag and improving tip flow. Reference 4 has a chapter on nonplanar lifting-surface theory, however, only lift curve-slope data of a V wing and near ground data are presented.

A recent theoretical parametric study of wing winglet configurations is made in reference 5. It is concluded in this reference that for the same root bending moment, a winglet provides a greater induced efficiency increment than does a tip extension. This study provides an abundance of winglet data with a wide range of geometric values of wing and winglet. A summary statement in reference 5 is 'This study provides sweeping confirmation, for a wide range of wings, of the recommendations of Whitcomb in NASA TN D-8260'. The winglet concept has been pioneered by Richard T. Whitcomb.

Present day design objectives are to interrelate aerodynamics with structural and weight characteristics and determine possible improvements in aerodynamic efficiency. As an example, a planar wing design is established. This wing has a certain root bending moment, lift, surface area, and induced drag. The designer determines that a wing winglet configuration with the same bending moment, lift, and surface area, has less induced drag. The designer may choose a highly staggered biplane winglet configuration with same as single wing structural weight, lift, and surface area, and determines that induced drag is the same, however, fuselage bending moment is greatly reduced with the staggered biplane configuration.

Objectives of the present study are to develop nonplanar wing loading methods which are viable for taking into account interference effects from other wings or from other vortex systems. Nonplanar means that a wing or vortex system extends vertically as well as laterally. Because nonplanar wing theory combined with other nonplanar vortex systems can become analytically complex and computationally limited, a nonplanar load line method will be developed. A planar wing load line theory is developed in reference 6. Load line theory is a lifting surface theory confined to a line, for arbitrary wing chord distribution, quasi two-dimensional, and solutions result in spanwise loading aerodynamics but no chord loading detail. This theory satisfies all boundary conditions along the span of the wing. Analytically, nonplanar load line principles can be made to extend and expand into nonplanar slender wing and elliptic wing analyses which, in addition, have a higher order of direct solution uniqueness. Nonplanar wing theory starts by developing generalized loading integral equations which relate the induced velocity normal to the surface to the wing loading, or a sum of wing loadings if for multiwings.

SYMBOLS

A	aspect ratio of nonplanar wing, $4s_e^2/S_e$
A_p	aspect ratio of planar wing, b_p^2/S
a_n, a_n*	Fourier coefficient of spanwise loading along the wing, equation (15)
b_p	wing span of planar wing
C_{D_i}	induced drag coefficient, D_i/qS_e, equation (69)
C_L	lift coefficient, L/qS_e, equation (54)

C_l	wing rolling moment coefficient, rolling moment/$qS_e 2s_e$, equation (61)
C_{mb_b}	wing running bending moment coefficient about lateral point η_b, $M_{b_b}/qS_e 2s_e$, equation (56)
C_{mb_r}	wing root bending moment coefficient, $M_{b_r}/qS_e 2s_e$
c	wing chord
c_{av}	wing average chord, $S_e/2s_e$
c_n, c_{n^*}	equals c_p with n or n* substituted for p
c_p	wing chord Fourier coefficients, equation (35)
$c_{\alpha n}$	Fourier coefficients for product of wing chord and angle of attack conditions, equation (35)
D_i	wing induced drag
D_{nn^*}	nonplanar induced drag influence coefficients, zero for planar wing, equation (67)
e	induced drag efficiency factor, equation (116)
G	dimensionless circulation, $\Gamma/2s_e V$, equation (14)
I_{nn^*}	wing chord influence coefficients, equation (35)
K_{nn^*}	nonplanar wing chord influence coefficients, zero for planar wing, equation (35)

k	surface loading factor, equation (24)
L	wing lift, also wing rolling moment, equation (61)
L_1	nonplanar wing lateral-vertical plane influence function, equation (32)
L_{n^*w}	L_1 integration nonplanar wing spanwise loading influence function, equation (33)
M	odd integer, number of terms in quadrature formula, equation (18)
M_b	wing bending moment about a specified span station
N	integer denoting number of unknowns and equations, equation (34)
n, n^*, p	integers of spanwise loading Fourier coefficients and influence coefficients, odd only for symmetric loading, equations (15), (34), and (35)
q	dynamic pressure, $\frac{1}{2}\rho V^2$
S_e	surface area of nonplanar wing, includes wing area in yz-plane
S_p	surface area of planar wing
s	spanwise coordinate along nonplanar wing surface, figure 1(a)
s_e	total semispan distance spanwise along wing surface from wing root to wing tip, figure 1(a)
V	free stream velocity

w	induced velocity normal to wing surface or trailing vorticity sheet, equations (5) or (6)
w	integers which denote span stations, equation (41)
y	lateral position of spanwise wing station s
z	vertical position of spanwise wing station s
α	aircraft angle of attack
α_c	wing geometry angle, equation (28)
α_i	induced angle normal to wing surface, equation (27)
Γ	wing circulation
γ	nonplanar wing dihedral cant angle, measured from y-axis, figure 1(a)
ε	wing twist angle
δ	dimensionless vertical coordinate, z/s_e
η	dimensionless lateral coordinate, y/s_e
η_b, ζ_b	spanwise station at which wing running bending moment is taken
η_{cp}	lateral semispanwise center of pressure location
θ, θ_o	angles used in derivation of induced velocity, figure 1(a)
λ	wing taper ratio, tip chord/root chord

λ_o, λ_w planar wing winglet taper ratios, equation (75)

λ_{wo} ratio of winglet root chord to wing root chord, equation (75)

Λ sweep angle of wing half chord line

μ integers for quadrature formula, equation (18)

ρ density

ϕ spanwise trigonometric coordinate, $\cos^{-1}\sigma$, equation (15)

σ dimensionless spanwise coordinate, s/s_e, equation (14)

ψ winglet toein angle, positive for toein deflection, equation (28)

Subscripts:

av average

b bending moment, also bending moment about lateral point η_b

cp center of pressure

e nonplanar wing tip

i, j ith and jth vorticity sheets, equation (6)

n,n*,p integers, equations (34) and (35)

o spanwise station where winglet begins, that is junction of wing and winglet

p	planar wing
r	wing root
v	vorticity sheet
w	normal to surface induced velocity or downwash point
w	integers, equations (41) and (71)
μ	integers, equations (18), (21), and (22)

DEVELOPMENT OF THEORY

Nonplanar loading theory differs from planar theory by the difference in velocity induced normal to the wing surfaces. In load line theory this induced velocity is simply that due to the trailing vorticity system. Using the nonplanar induced velocity combined with the planar load-line theory of reference 6 will provide a nonplanar load-line theory.

Induced Velocity Integral Equation of Nonplanar Vorticity Sheet

Single vorticity sheet. - A single nonplanar trailing sheet extending longitudinally from zero to infinity is shown in figure 1(a). The normal induced velocity at point (y_w, z_w), by Biot-Savart law, is given by

$$\left.\begin{aligned} dw(y_w,z_w) &= \frac{-d\Gamma}{4\pi r}\cos\theta \\ \text{where} \quad r &= [(y_v - y_w)^2 + (z_v - z_w)^2]^{1/2} \end{aligned}\right\} \tag{1}$$

Referring to figure 1(a), the following relations can be developed:

$$\left.\begin{aligned} &\theta + \frac{\pi}{2} + \gamma_w = \frac{\pi}{2} + \theta_0, \quad \theta = \theta_0 - \gamma_w \\ &\cos\gamma_w = \cos\theta_0\cos\gamma_w + \sin\theta_0\sin\gamma_w \\ &\cos\theta_0 = (y_v - y_w)/r, \quad \sin\theta_0 = (z_v - z_w)/r \\ &\tan\gamma_w = \left(\frac{dz}{dy}\right)_w, \quad \cos\gamma_w = \left[1 + \left(\frac{dz}{dy}\right)_w^2\right]^{-1/2}, \quad \sin\gamma_w = \left(\frac{dz}{dy}\right)_w\left[1 + \left(\frac{dz}{dy}\right)_w^2\right]^{-1/2} \end{aligned}\right\} \tag{2}$$

Let s be distance along the surface of the vorticity sheet measured from midpoint of the sheet. Then the differential relation between s and y is

$$ds = \left[1 + \left(\frac{dz}{dy}\right)^2\right]^{1/2} dy \tag{3}$$

With the θ, θ_0, and γ_w values of equation (2) inserted into equation (1), the incremental downwash at point y_w, z_w due to a nonplanar trailing vorticity sheet is

$$\begin{aligned} dw(y_w,z_w) &= -\frac{\cos\gamma_w}{4\pi r^2}\left[y_v - y_w + (z_v - z_w)\tan\gamma_w\right]\frac{d\Gamma}{ds}\,ds \\ &= -\frac{1}{4\pi}\left[1 + \left(\frac{dz}{dy}\right)_w^2\right]^{-1/2} \frac{y_v-y_w + (z_v-z_w)\left(\frac{dz}{dy}\right)_w}{(y_v-y_w)^2 + (z_v-z_w)^2}\frac{d\Gamma}{ds}\,ds \end{aligned} \tag{4}$$

Integration of equation (4) leads to

$$w(y_w,z_w) = -\frac{1}{4\pi}\left[1 + \left(\frac{dz}{dy}\right)_w^2\right]^{-1/2}\int_{-s_e}^{s_e} \frac{y_v-y_w+(z_v-z_w)\left(\frac{dz}{dy}\right)_w}{(y_v-y_w)^2 + (z_v-z_w)^2}\frac{d\Gamma}{ds}\,ds \tag{5}$$

where the integration is taken along s, that is a line integral along the vorticity sheet. The integrand variable y_v is related with s by the expression given in equation (3). The point at which normal velocity w is determined is defined by y_w and z_w. The nonplanar vertical displacement of the wing given by z is an arbitrary function of y. The derivative $(dz/dy)_w$ is the slope at z at the point y_w, z_w, and is constant in the integrand of equation (5) as are also y_w and z_w.

Multiple vorticity sheets. - An example of a pair of vorticity sheets is shown in figure 1(b). The total induced normal velocity at sheet j is not only that due to sheet j but also that due to sheet i, or for many sheets with i = 1, 2, . . . In equation (5) the induced velocity normal to the slope line $(dz/dy)_w$ is determined at point (y_w, z_w) which is a point on the vorticity sheet represented by the function $z_v(y)$. However, the point (y_w, z_w) is arbitrary and can be on any curve z(y), that is can be different than the $z_v(y)$ curve. Let z_{vi} represent an N-group of vorticity sheet curves, then the normal velocity along the z_{wj} curve obtained by reapplication of equation (5) is given by

$$w_j(y_{wj},z_{wj}) = \frac{-1}{4\pi}\left[1 + \left(\frac{dz}{dy}\right)_{wj}^2\right]^{-\frac{1}{2}}\sum_{i=1}^{N}\left[\int_{-s_{ei}}^{s_{ei}} \frac{y_{vi}-y_{wj}+(z_{vi}-z_{wj})\left(\frac{dz}{dy}\right)_{wj}}{(y_{vi}-y_{wj})^2 + (z_{vi}-z_{wj})^2}\frac{d\Gamma_i}{ds_{vi}}\,ds_{vi}\right] \tag{6}$$

where j = 1 through N. With equation (6) the induced normal velocity can be determined along the span of N abitrarily shaped vorticity sheets or wings. Some examples of various shapes that can be analyzed are shown as follows:

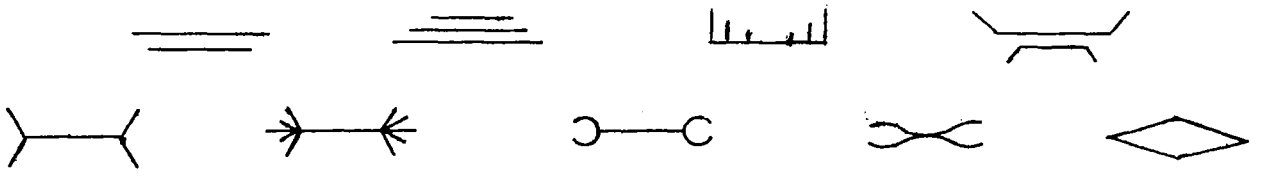

Induced Velocity of Wing with Winglet

For a single wing with winglet the vorticity sheet appears as follows:

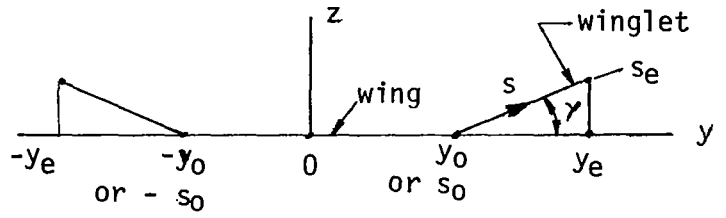

For this nonplanar geometry the coordinate relations are

in the range	in the range	in the range
$-y_0 \leq y \leq y_0$	$y_0 \leq y \leq y_e$	$-y_e \leq y \leq -y_0$
$z = 0$	$z = (y-y_0)\tan\gamma$	$z = (-y-y_0)\tan\gamma$
$\frac{dz}{dy} = 0$	$\frac{dz}{dy} = \tan\gamma$	$\frac{dz}{dy} = -\tan\gamma$
$y = s$	$y = s_0 + (s-s_0)\cos\gamma$	$y = -s_0+(s+s_0)\cos\gamma$
	$z = (s - s_0)\sin\gamma$	$z = -(s+s_0)\sin\gamma$

(7)

With equation (7) values inserted into equation (5) the velocity normal to the surface is given by

for $0 \leq s_w \leq s$

$$w(s_w) = -\frac{1}{4\pi}\int_{-s_o}^{s_o} \frac{\frac{d\Gamma}{ds_v}\,ds_v}{s_v - s_w} - \frac{1}{4\pi}\int_{-s_o}^{s_e} \frac{[s_v\cos\gamma - s_w + s_o(1-\cos\gamma)]\frac{d\Gamma}{ds_v}\,ds_v}{[s_v\cos\gamma - s_w + s_o(1-\cos\gamma)]^2 + (s_v - s_o)^2\sin^2\gamma}$$

$$- \frac{1}{4\pi}\int_{-s_e}^{-s_o} \frac{[s_v\cos\gamma - s_w - s_o(1-\cos\gamma)]\frac{d\Gamma}{ds_v}\,ds_v}{[s_v\cos\gamma - s_w - s_o(1-\cos\gamma)]^2 (s_v + s_o)^2\sin^2\gamma} \qquad (8)$$

and for $s_o \leq s_w \leq s_e$

$$w(s_w) = -\frac{1}{4\pi}\int_{-s_o}^{s_o} \frac{[s_v\cos\gamma - s_w + s_o(1-\cos\gamma)]\frac{d\Gamma}{ds_v}\,ds_v}{[s_v - s_w\cos\gamma - s_o(1-\cos\gamma)]^2 + (s_w - s_o)^2\sin^2\gamma} - \frac{1}{4\pi}\int_{s_o}^{s_e} \frac{\frac{d\Gamma}{ds_v}\,ds_v}{s_v - s_w}$$

$$- \frac{1}{4\pi}\int_{-s_e}^{-s_o} \frac{[-(1-2\cos^2\gamma)s_v - s_w - 2s_o(1-\cos\gamma)\cos\gamma]\frac{d\Gamma}{ds_v}\,ds_v}{[(s_v - s_w)\cos\gamma - 2s_o(1-\cos\gamma)]^2 + (s_v + s_w)^2\sin^2\gamma} \qquad (9)$$

The integral with the $(s_v - s_w)^{-1}$ term in the integrand contributes a large part of the induced velocity, because it results from the vorticity nearest the point at which the velocity is determined. This integral is analytically simple to obtain if the integration is taken over the whole wing; that is, from $-s_e$ to s_e. Equations (8) and (9) give the same result if the $(s_v - s_w)^{-1}$ integral is added for extending the integration and subtracted from the more complicated integrand. With this adding and subtracting and in dimensionless notation, equations (8) and (9) simplify to

for $0 \leq \sigma_w \leq \sigma_o$

$$\alpha_i(\sigma_w) = -\frac{1}{2\pi}\int_{-1}^{1} \frac{\frac{dG}{d\sigma_v}\,d\sigma_v}{\sigma_v - \sigma_w} - \frac{1}{2\pi}\int_{\sigma_o}^{1} L_- \frac{dG}{d\sigma_v}\,d\sigma_v - \frac{1}{2\pi}\int_{-1}^{-\sigma_o} L_+ \frac{dG}{d\sigma_v}\,d\sigma_v \qquad (10)$$

and for $\sigma_o \leq \sigma_w \leq 1$

$$\alpha_i(\sigma_w) = \frac{-1}{2\pi}\int_{-1}^{1} \frac{\frac{dG}{d\sigma_v}\, d\sigma_v}{\sigma_v - \sigma_w} - \frac{1}{2\pi}\int_{-\sigma_o}^{\sigma_o} L_- \frac{dG}{d\sigma_v}\, d\sigma_v - \frac{1}{2\pi}\int_{-1}^{-\sigma_o} L_o \frac{dG}{d\sigma_v}\, d\sigma_v \tag{11}$$

where

$$L_\pm = - \frac{(\sigma_v \pm \sigma_o)(\sigma_v + \sigma_w \pm 2\sigma_o)(1 - \cos\gamma)}{[(\sigma_v-\sigma_w)^2 + 2(\sigma_v \pm \sigma_o)(\sigma_w \pm \sigma_o)(1-\cos\gamma)]\,(\sigma_v-\sigma_w)} \tag{12}$$

$$L_o = -\frac{(1-2\cos^2\gamma)\sigma_v + \sigma_w + 2\sigma_o\,(1-\cos\gamma)\cos\gamma}{[(\sigma_v-\sigma_w)\cos\gamma - 2\sigma_o\,(1-\cos\gamma)]^2 + (\sigma_v+\sigma_w)^2\sin^2\gamma} - \frac{1}{\sigma_v - \sigma_w} \tag{13}$$

The dimensionless values in equations (10) through (13) are defined as follows:

$$\sigma = \frac{s}{s_e}\,, \quad \sigma_o = \frac{s_o}{s_e}\,, \quad G = \frac{\Gamma}{2s_eV}\,, \quad \alpha_i = \frac{w}{V} \tag{14}$$

With equations (10) and (11) the induced angle normal to the nonplanar wing surface can be determined for an arbitrary loading G. This is for the nonplanar wing or wing-winglet defined in equation (7).

Integration with G represented by a Fourier series. - Let the wing loading coefficient along the s or σ coordinate of the wing be given by

$$G(\phi) = \sum_{n=1}^{N} a_n \sin n\phi\,, \quad \frac{dG}{d\phi} = \sum_{n=1}^{N} n\, a_n \cos n\phi \tag{15}$$

where $\sigma = \cos\phi$. Then the first integral in equations (10) and (11) becomes

$$-\frac{1}{2\pi}\int_{-1}^{1} \frac{\frac{dG}{d\sigma_v}\, d\sigma_v}{\sigma_v - \sigma_w} = \frac{1}{2\pi}\int_{0}^{\pi} \frac{\frac{dG}{d\phi_v}\, d\phi_v}{\cos\phi_v - \cos\phi_w} = \frac{1}{2\pi}\sum_{n=1}^{N} n\, a_n \int_{0}^{\pi} \frac{\cos n\phi_v\, d\phi_v}{\cos\phi_v - \cos\phi_w}$$

Since

$$\int_{0}^{\pi} \frac{\cos n\phi_v\, d\phi_v}{\cos\phi_v - \cos\phi_w} = \frac{\pi \sin n\phi_w}{\sin\phi_w} \tag{16}$$

then

$$-\frac{1}{2\pi}\int_{-1}^{1}\frac{\frac{dG}{d\sigma_v}\,d\sigma_v}{\sigma_v-\sigma_w}=\frac{1}{2\sin\phi_w}\sum_{n=1}^{N}n\,a_n\sin n\phi_w \tag{17}$$

When G is expanded in a Fourier series the L integrals become complicated; however accurate integrations can be obtained by using a simple quadrature formula given by

$$\int_{\phi_1}^{\phi_2}f(\phi)d\phi=\frac{\phi_2-\phi_1}{M+1}\left[\frac{f(\phi_1)+f(\phi_2)}{2}+\sum_{\mu=1}^{M}f(\phi_\mu)\right] \tag{18}$$

where $\phi_\mu=\phi_1+\frac{\mu(\phi_2-\phi_1)}{M+1}$, and M is an odd integer. Then the L_- integral of equation (10) becomes

$$-\frac{1}{2\pi}\int_{\sigma_o}^{1}L_-\frac{dG}{d\sigma_v}\,d\sigma_v=\frac{1}{2\pi}\int_{0}^{\phi_o}L_-(\phi_v,\phi_w)\frac{dG}{d\phi_v}\,d\phi_v=\frac{1}{2\pi}\sum_{n=1}^{N}n\,a_n\int_{0}^{\phi_o}L_-(\phi_v,\phi_w)\cos n\phi_v\,d\phi_v$$

$$=\sum_{n=1}^{N}n\,a_n\left\{\frac{\phi_o}{4\pi(M_1+1)}\left[L_-(0,\phi_w)+L_-(\phi_o,\phi_w)\cos n\phi_o+2\sum_{\mu=1}^{M_1}L_-(\phi_{1\mu},\phi_w)\cos n\phi_{1\mu}\right]\right\} \tag{19}$$

where $\phi_{1\mu}=\frac{\mu\phi_o}{M_1+1}$, and where examination of equation (12) shows that $L_-(\phi_o,\phi_w)=0$. Similar integrations are made for the other L integrals which appear in equations (10) and (11). With the equation (19) procedure and with equation (17), equations (10) and (11) for symmetrical loading (n = odd) reduce to

$$\alpha_i(\phi_w)=\sum_{\substack{n=1\\ \text{odd}}}^{N}n\,a_n\left(\frac{\sin n\phi_w}{2\sin\phi_w}+L_{nw}\right) \tag{20}$$

where for $0 \leq \sigma_w \leq \sigma_o$ or $\phi_o \leq \phi_w \leq \frac{\pi}{2}$

$$L_{nw} = \frac{\phi_o}{2\pi(M_1+1)}\left[\frac{L_-(o,\phi_w)}{2} + \sum_{\mu=1}^{M_1} L_-(\phi_{1\mu},\phi_w)\cos n\phi_{1\mu}\right] + \frac{\phi_o}{2\pi(M_2+1)}\left[\frac{-L_+(\pi,\phi_w)}{2} + \sum_{\mu=1}^{M_2} L_+(\phi_{2\mu},\phi_w)\cos n\phi_{2\mu}\right] \tag{21}$$

where $\phi_{1\mu} = \frac{\mu\phi_o}{M_1+1}$, $\phi_{2\mu} = \pi - \frac{\mu\phi_o}{M_2+1}$

and for $\sigma_o \leq \sigma_w \leq 1$ or $0 \leq \phi_w \leq \phi_o$

$$L_{nw} = \frac{\pi-2\phi_o}{2\pi(M_3+1)}\left[\frac{-L_-(\pi-\phi_o,\phi_w)\cos n\phi_o}{2} + \sum_{\mu=1}^{M_3} L_-(\phi_{3\mu},\phi_w)\cos n\phi_{3\mu}\right] + \frac{\phi_o}{2\pi(M_4+1)}\left[\frac{-L_o(\pi,\phi_w)}{2} + \sum_{\mu=1}^{M_4} L_o(\phi_{4\mu},\phi_w)\cos n\phi_{4\mu}\right] \tag{22}$$

where $\phi_{3\mu} = \phi_o + \frac{\mu(\pi-2\phi_o)}{M_3+1}$, $\phi_{4\mu} = \pi - \frac{\phi_o}{M_4+1}$, and M_1, M_2, M_3, and M_4 are odd integers.

In equations (21) and (22), the $L_+(\phi_\mu,\phi_w)$ and $L_o(\phi_\mu,\phi_w)$ functions are given by equations (12) and (13), in which $\sigma_v = \cos\phi_\mu$, $\sigma_w = \cos\phi_w$, and $\sigma_o = \cos\phi_o$.

Load-Line Theory

Load-line theory is developed in reference 6 for the planar wing. In this theory the boundary conditions are satisfied at all points along the span and an aspect ratio factor is introduced, however, the theoretical simplicity of the lifting-line method is maintained. In the present development, this load-line theory is extended into a load-line theory for nonplanar wings.

The integral loading equations start with the relation that section loading is given by

$$\left.\begin{aligned} \rho V\Gamma &= 2\pi\ (\alpha_c - k\alpha_i)qc \\ \text{or} \qquad \frac{\Gamma}{V} &= \pi c\ (\alpha_c - k\alpha_i) \end{aligned}\right\} \tag{23}$$

where α_c is the incidence angle between free stream velocity and wing chord, α_i is the induced angle due to wing wake vorticity sheet or multiple vorticity sheets extending longitudinally from zero to infinity, and k is a lifting surface downwash factor developed in reference 6. The factor k originated in the study presented in reference 7, where it had the value $(A + 4)/(A + 2)$. Later work showed that a more accurate value for k is

$$k = \frac{A + 3.79}{A + 1.895} \tag{24}$$

Using the dimensionless definitions of equations (14) and (15) and defining nonplanar aspect ratio and average wing chord as

$$\left.\begin{aligned} A = \frac{4s_e{}^2}{S_e},\ c_{av} = \frac{S_e}{2s_e},\ & S_e = \text{surface area of nonplanar wing} \\ & 2s_e = \text{wing tip to tip perimeter length} \end{aligned}\right\} \tag{25}$$

then equation (23) becomes

$$\sum_{n=1}^{N} a_n \sin n\phi = \frac{\pi}{A}\frac{c}{c_{av}}(\alpha_c - k\alpha_i) \tag{26}$$

Equation (26) is the form of the equation for lifting-line theory solutions except here the k factor is introduced. In lifting-line theory k=1. The planform geometry terms c/c_{av} and α_c are functions of ϕ, and $\alpha_i = \alpha_i(\phi, n, a_n)$. By specifying ϕ at m spanwise stations, m linear simultaneous equations result with m unknown a_n's. These are solved for a_n. These values of a_n represent the solution for which the boundary conditions are satisfied at a finite m spanwise stations.

In load-line theory the boundary conditions are satisfied at all points along the wing span. This is possible by a spanwise integration of the wing chord, angle of attack, and induced angle. In equation (26) α_i can be represented by the function

$$\alpha_i = \alpha_i \ (\phi, n^*, a_n^*)$$

Then the expression on the right side of equation (26) is only a function of ϕ and n^* but not of n. Then by Fourier theory the Fourier coefficients are given by

$$a_n = \frac{1}{2\pi}\int_0^{\pi}\left\{\frac{\pi}{A}\frac{c}{c_{av}}\left[\alpha_c - k\alpha_i(\phi, n^*, a_n^*)\right]\right\} \sin n\phi \ \ d\phi$$

or

$$a_n = \frac{2}{A}\int_0^{\pi} \frac{c}{c_{av}} \alpha_c \sin n\phi \ \ d\phi - \frac{2k}{A}\int_0^{\pi} \frac{c}{c_{av}} \alpha_i \ (\phi, n^*, a_n^*) \sin n\phi \ d\phi \qquad (27)$$

for n = 1, 2, 3, . . .

For a single wing, α_i in equation (27) is given by the ratio of equation (5) to V. For multiple wings, α_c in equation (27) is added to equation (6) minus equation (5). In addition, all the terms in equation (27) become those for the jth wing; that is, A_j, $(c/c_{av})_j$, α_{cj}, k_j, and a_{jn}, which are the Fourier loading coefficients for the jth wing. The wing geometry angle α_c is made up of the effect of wing or aircraft angle of attack α on the nonplanar wing, the wing twist ε, and the toein-toeout angle ψ of the nonplanar wing. Wing twist and toein angle with the wing uninclined are defined as angles between the wing chord and free stream velocity, positive in the direction for loading increasing on the upper wing surface. For the nonplanar wing the effective angle of attack at a wing section is $\alpha \cos \gamma$. Then

$$\left.\begin{aligned} \alpha_c &= \alpha \cos \gamma + \varepsilon + \psi \\ \text{where } \tan \gamma &= \left(\frac{d\zeta}{d\eta}\right)_\phi, \ \cos \gamma = \left[1 + \left(\frac{d\zeta}{d\eta}\right)_\phi^2\right]^{-1/2} \\ \text{and} \qquad \varepsilon &= \varepsilon(\phi), \quad \psi = \psi(\phi) \end{aligned}\right\} \qquad (28)$$

Thus the solution of the nonplanar wing loading integral equation reduces to the load-line solution for determining the a_n Fourier loading coefficients of equation (27). It is simply a wing geometry integration which includes the wing chord distribution along σ or ϕ and the angle α_c distribution given in equation (28). The second integral involves the integration of $w\ (y_w, z_w) = V\alpha_i(\phi_w)$ of equation (5). In a dimensionless equation (5) the nondimensional derivative of circulation becomes an n* series given by equation (15) but with $n = n^*$, and $\phi = \phi_v$.

Load-line method for single wing. - The induced angle in equation (27) can be expressed as that due to a planar wing plus that due to the difference between nonplanar and planar wings, as was done in equations (10) and (11). Let α_{ip} represent the induced angle due to a planar wing and α_{io} that due the effects of the nonplanar condition. Then $\alpha_i = \alpha_{ip} + \alpha_{io}$. Then, in nondimensional terms, equation (5) can be written as

$$\alpha_i\ (\phi_w) = \alpha_{ip}\ (\phi_w) + \alpha_{io}\ (\phi_w) \tag{29}$$

where with equation (17)

$$\alpha_{ip}\ (\phi_w) = -\frac{1}{2\pi}\int_{-1}^{1} \frac{\frac{dG}{d\sigma_v}\, d\sigma_v}{\sigma_v - \sigma_w} = \sum_{n^*=1}^{N} \frac{n^* a_{n^*} \sin n^* \phi_w}{2 \sin \phi_w} \tag{30}$$

and with equation (15)

$$\alpha_{io}\ (\phi_w) = \frac{-1}{2\pi}\int_{-1}^{1} L_1 \frac{dG}{d\sigma_v}\, d\sigma_v = \sum_{n^*=1}^{N} n^* a_{n^*} L_{n^*w} \tag{31}$$

where

$$L_1 = \frac{\eta_v - \eta_w + (\zeta_v - \zeta_w)\left(\frac{d\zeta}{d\eta}\right)_w}{\left[1 + \left(\frac{d\zeta}{d\eta}\right)_w^2\right]^{1/2}\left[(\eta_v - \eta_w)^2 + (\zeta_v - \zeta_w)^2\right]} - \frac{1}{\sigma_v - \sigma_w} \tag{32}$$

which approaches zero as $\eta_v \to \eta_w$

$$L_{n^*w} = \frac{1}{2\pi}\int_0^{\pi} L_1 \cos n^* \phi_v \, d\phi_v$$

$\eta = y/s_e$, $\zeta = z/s_e$, $\sigma = s/s_e = \cos\phi$, and η, ζ, and σ by equation (3) are related by $d\sigma = \left[1 + \left(\frac{d\zeta}{d\eta}\right)^2\right]^{1/2} d\eta$ (33)

With equations (29), (30), and (31) inserted into equation (27), the loading integral equation for the single nonplanar wing becomes

$$a_n = \frac{\pi}{A} c_{\alpha n} - \frac{\pi k}{2A} \sum_{n^*=1}^{N} n^* I_{nn^*} a_{n^*} - \frac{\pi k}{A} \sum_{n^*=1}^{N} n^* K_{nn^*} a_{n^*} \qquad (34)$$

$n = 1, 2, 3, \ldots\ldots N$

where

$$c_{\alpha n} = \frac{2}{\pi}\int_0^{\pi} \frac{c}{c_{av}} \alpha_c \sin n\phi \, d\phi$$

$$I_{nn^*} = \frac{2}{\pi}\int_0^{\pi} \frac{c}{c_{av}} \frac{\sin n^*\phi}{\sin \phi} \sin n\phi \, d\phi = \sum_{p=|n-n^*|+1}^{n+n^*-1} c_p$$

$$c_p = \frac{2}{\pi}\int_0^{\pi} \frac{c}{c_{av}} \sin p\phi \, d\phi \overset{p=1}{=} \frac{4}{\pi}$$

$$K_{nn^*} = \frac{2}{\pi}\int_0^{\pi} \frac{c}{c_{av}} L_{n^*w} \sin n\phi \, d\phi \qquad (35)$$

where the $I_{nn^*} - c_p$ relation is derived in reference 6. The first two terms on the right side of equation (34) are the same as those for the planar wing since then $K_{nn^*} = 0$ because $L_1 = 0$. The solution for a_n involves N equations and N unknowns of a_n or a_{n^*} which are solved as linear simultaneous

equations. The coefficients c_p and $c_{\alpha n}$ are integrations of the boundary conditions, that is, the wing chord distribution and wing angle of attack distribution along the spanwise $\phi = \cos^{-1} \sigma$ parameter. The c_p's are the Fourier coefficients of the wing planform which wing in a Fourier series function can be represented by

$$\frac{c(\phi)}{c_{av}} = \sum_{p=1}^{\infty} c_p \sin p\phi \tag{36}$$

Similarly $c_{\alpha n}$'s are the Fourier coefficients for the product of wing chord and geometric angle α_c. The angle α_c which the wing chord makes with free stream velocity is given in equation (28) where α is constant with respect to ϕ or σ. Equation (34) applies to a single nonplanar wing of any vertical-lateral shape since $\zeta = \zeta(\eta)$ or $z = z(y)$ are arbitrary functions. In addition, the wing chord distribution with unswept midchord line can be for any planform shape, and the wing twist or winglet angle distribution are arbitrary functions.

Symmetric spanwise loading. - This loading results from a spanwise symmetric wing planform with spanwise symmetric distribution of angle of attack across the span. With these conditions only odd numbered values of p, n, and n* of c_p, $c_{\alpha n}$, and K_{nn*} have values in equation (35). For symmetric loading solutions it is convenient to evaluate the a_1 coefficient in terms of ratios of a_n/a_1. For n = 1 equation (34) becomes

$$a_n = \frac{\pi}{A} c_{\alpha 1} - \frac{\pi k}{2A} I_{11} a_1 - \frac{\pi k}{A} K_{11} a_1 - \frac{\pi k}{2A} \sum_{\substack{n^*=3 \\ \text{odd}}}^{N} n^* I_{1n^*} a_{n^*} - \frac{\pi k}{A} \sum_{\substack{n^*=3 \\ \text{odd}}}^{N} n^* K_{1n^*} a_{n^*} \tag{37}$$

Since $I_{11} = \frac{4}{\pi}$, $I_{1n^*} = c_{n^*}$, $I_{n1} = c_n$

then

$$a_1 = \frac{\pi c_{\alpha 1}}{A + 2k \left[1 + \frac{\pi}{2} K_{11} + \frac{\pi}{4} \sum_{\substack{n^*=3 \\ \text{odd}}}^{N} (c_{n^*} + 2K_{1n^*}) n^* \frac{a_{n^*}}{a_1}\right]} \tag{38}$$

Dividing equation (34) by equation (38) gives

$$\frac{a_n}{a_1} = \frac{c_{\alpha n}}{c_{\alpha 1}}\left[1+\frac{2k}{A}\left(1+\frac{\pi}{2}K_{11}\right)\right] - \frac{\pi k}{2A}\left(c_n+2K_{n1}\right)+ \frac{\pi k}{2A}\sum_{\substack{n^*=3\\ \text{odd}}}^{N}\left[\frac{c_{\alpha n}}{c_{\alpha 1}}\left(c_{n^*}+2K_{1n^*}\right)-I_{nn^*}-2K_{nn^*}\right]n^*\,\frac{a_n}{a_1} \tag{39}$$

for $n = 3, 5, 7, \ldots N$

where the coefficients $c_{\alpha n}$, I_{nn^*}, K_{nn^*}, and c_p (note that p can be substituted by n or n* in the c_p integral) are given in equation (35). Only the coefficients for odd numbered values of n, n*, and p are needed for the symmetric loading solution. Equation (39) has (N-1)/2 equations in n with (N-1)/2 unknowns of a_n/a_1 or a_{n^*}/a_1 which are evaluated by solving as simultaneous linear equations. The c_n and c_{n^*} coefficients are the c_p values given in equation (33) but with n or n* substituted for p.

Planar-wing winglet solution for symmetric spanwise loading. - The Fourier loading coefficients a_n are obtained from the solution of equations (39) and (38). For this nonplanar configuration the L_1 function of equation (32) is formulated as $L_{\pm}$ and L_o functions given in equations (12) and (13). The numerical integration of these functions results in the L_{nw} expressions given in equations (21) and (22). From equation (35) the K_{nn^*} coefficients are

$$K_{nn^*} = \frac{2}{\pi}\int_0^{\pi}\frac{c}{c_{av}}\,L_{n^*w}\,\sin n\phi\,d\phi \tag{40}$$

where for this nonplanar configuration the L_{n^*w} are given by L_{nw} of equations (21) and (22) but with the substitution of n* for n. Equation (40) can be integrated numerically by using the quadrature formula of equation (18). Let $\phi = \phi_w = w\pi/(M+1)$, then

$$K_{nn^*} = \frac{2}{M+1}\sum_{w=1}^{M}\left[\left(\frac{c}{c_{av}}\right)_w L_{n^*w}\,\sin n\phi_w\right]$$

where M is an odd integer. Since the chord distribution spanwise is symmetric and for odd n sin $n\phi_w$ is symmetric, and the induced angle contribution of L_{n^*w} is symmetric, then

$$K_{nn^*} = \frac{2}{M+1}\left[\left(\frac{c}{c_{av}}\right)_{\frac{M+1}{2}} L_{n^*\,\frac{M+1}{2}} \sin n\,\frac{\pi}{2} + 2\sum_{w=1}^{\frac{M-1}{2}} \left(\frac{c}{c_{av}}\right)_w L_{n^*w} \sin n\phi_w\right] \quad (41)$$

where the (M+1)/2 subscript denotes midwing conditions, that is at $\phi_w = \pi/2$ or $\sigma_w = \cos\phi_w = 0$. The chord term $(c/c_{av})_w$ is that at span station $\phi_w = w\pi/(M+1)$. L_{n^*w} is with ϕ_w in the ϕ_w range of equations (21) or (22), in which n is changed to n*. In equations (12) and (13) $\sigma_w = \cos[w\pi/(M+1)]$. To minimize numerical integration error ϕ_o should be chosen between the ϕ_w points, or $\phi_o \neq w\pi/(M+1)$.

The planar-wing winglet a_n coefficients for symmetric spanwise loading are obtained by the solution of equation (39) with the K_{nn^*} of equation (41) and the $c_{\alpha n}$, I_{nn^*}, and c_p of odd n, n*, p integers in equation (35). Example values of L_{n^*w} with $\phi_o = 5\pi/32$ radians have been computed using equations (21) and (22) and are presented in table I. These values are for M = 15 with $\phi_w = w\pi/16$.

Slender Wing Theory and Elliptic Wing Theory

Elliptic wing and A→∞ limit solution. - For the elliptic wing

$$\left.\begin{aligned} c &= c_r\,(1-\sigma^2)^{1/2} = c_r \sin\phi, \quad S_e = \frac{\pi}{2} c_r s_e, \quad \frac{c_r}{2s_e} = \frac{4}{\pi A} \\ c_{av} &= \frac{S_e}{2s_e} = \frac{\pi}{4} c_r, \quad \frac{c}{c_{av}} = \frac{4}{\pi}(1-\sigma^2)^{1/2} = \frac{4}{\pi}\sin\phi \end{aligned}\right\} \quad (42)$$

With this c/c_{av} equations (26), (29), (30), and (31) are combined to give

$$\sum_{n=1}^{N} (A + 2nk)\, a_n \sin n\phi = 4\alpha_c \sin\phi - 4k \sum_{n^*=1}^{N} n^*\, a_{n^*} L_{n^*w} \sin\phi \quad (43)$$

then the Fourier loading coefficients for the elliptic wing planform are

$$a_n = \frac{\pi}{A+2nk}\left(c_{\alpha n} - k\sum_{n^*=1}^{N} n^* K_{nn^*}\, a_{n^*}\right) \qquad (44)$$

$$\text{for } n = 1, 2, \ldots N$$

where $c_{\alpha n}$ and K_{nn^*} are the coefficients given in equation (35) but with $c/c_{av} = (4/\pi)\sin\phi$, that is

$$c_{\alpha n} = \frac{8}{\pi^2}\int_0^{\pi} \alpha_c \sin\phi \sin n\phi \, d\phi, \quad K_{nn^*} = \frac{8}{\pi^2}\int_0^{\pi} L_{n^* w} \sin\phi \sin n\phi \, d\phi \qquad (45)$$

For symmetric loading on the elliptic planform, equation (44) becomes

$$\left.\begin{aligned} a_1 &= \frac{\pi c_{\alpha 1}}{A + 2k\left(1 + \frac{\pi}{2}K_{11} + \frac{\pi}{2}\sum_{\substack{n^*=3 \\ \text{odd}}}^{N} n^* K_{1n^*}\frac{a_{n^*}}{a_1}\right)} \\ \frac{a_n}{a_1} &= \frac{1}{A+2nk}\left[A\frac{c_{\alpha n}}{c_{\alpha 1}} + \pi k\left(\frac{2}{\pi}\frac{c_{\alpha n}}{c_{\alpha 1}} + \frac{c_{\alpha n}}{c_{\alpha 1}}K_{11} - K_{n1}\right) + \pi k\sum_{\substack{n^*=3 \\ \text{odd}}}^{N}\left(\frac{c_{\alpha n}}{c_{\alpha 1}}K_{1n^*} - K_{nn^*}\right)n^*\frac{a_{n^*}}{a_1}\right] \\ &\text{for } n = 3, 5, \ldots N \end{aligned}\right\} \qquad (46)$$

As aspect ratio approaches infinity, the solutions for a_n reduce to direct relations between a_n and the wing geometry coefficient $c_{\alpha n}$. For $A \to \infty$ equations (38) and (39) become

$$\left.\begin{aligned} a_1 &\to \frac{\pi c_{\alpha 1}}{A} \\ \frac{a_n}{a_1} &\to \frac{c_{\alpha n}}{c_{\alpha 1}} \end{aligned}\right\} \qquad (47)$$

where $c_{\alpha n}$ is given in equation (35), or for the elliptic wing by equation (45).

Slender wing. - When aspect ratio approaches zero, then, for any wing planform with trailing edge cutout aft of all points of swept leading edge, as shown in reference 8, equation (44) for $A \to 0$, $k \to 2$, becomes

$$a_n = \frac{\pi}{4n}\left(c_{\alpha n} - 2\sum_{n^*=1}^{N} n^* K_{nn^*} a_{n^*}\right), \quad n = 1, 2, \ldots N \tag{48}$$

where $c_{\alpha n}$ and K_{nn^*} are given in equation (45). With symmetric loading equation (46) for a $A \to 0$ wing is

$$\left.\begin{aligned} a_1 &= \frac{\pi c_{\alpha 1}}{4 + 2\pi K_{11} + 2\pi \sum_{\substack{n^*=3 \\ \text{odd}}}^{N} n^* K_{1n^*} \frac{a_{n^*}}{a}} \\ \frac{a_n}{a_1} &= \frac{\pi}{2n}\left(\frac{2}{\pi}\frac{c_{\alpha n}}{c_{\alpha 1}} + \frac{c_{\alpha n}}{c_{\alpha 1}} K_{11} - K_{n1}\right) + \frac{\pi}{2n}\sum_{\substack{n^*=3 \\ \text{odd}}}^{N}\left(\frac{c_{\alpha n}}{c_{\alpha 1}} K_{1n^*} - K_{nn^*}\right) n^* \frac{a_{n^*}}{a} \end{aligned}\right\} \tag{49}$$

for $n = 3, 5, \ldots N$

Another derivation of nonplanar slender wing theory is to note from equation (26) that the boundary conditions are simply that $\alpha_c = k\alpha_i = 2\alpha_i$ as $A \to 0$. From equations (29), (30), and (31)

$$\alpha_i = \frac{1}{2 \sin \phi}\sum_{n=1}^{N} n\, a_n \sin n\phi + \sum_{n^*=1}^{N} n^* a_{n^*} L_{n^* w} \tag{50}$$

then, with the condition $\alpha_c = 2\alpha_i$, equation (50) can be written as

$$\sum_{n=1}^{N} n\, a_n \sin n\,\phi = \alpha_c \sin\phi - 2\sum_{n^*=1}^{N} n^* a_{n^*} L_{n^* w} \sin\phi$$

from which the Fourier coefficients are

$$na_n = \frac{2}{\pi}\int_0^{\pi} \alpha_c \sin\phi \sin n\phi \, d\phi - 2\sum_{n^*=1}^{N} n^* a_{n^*}\left(\frac{2}{\pi}\int_0^{\pi} L_{n^* w} \sin\phi \sin n\phi \, d\phi\right)$$

which in terms of $c_{\alpha n}$ and K_{nn^*} of equation (45), becomes

$$a_n = \frac{\pi}{4n}\left(c_{\alpha n} - 2\sum_{n^*=1}^{N} n^* K_{nn^*} a_{n^*}\right), \quad n = 1, 2, \ldots N \tag{51}$$

which is the same as that of equation (48).

Force and Moment Coefficients

Spanwise loading and lift coefficient. - With the Fourier loading coefficients a_n determined by equation (15), the spanwise loading distribution along the spanwise σ or ϕ coordinate is

$$G = \frac{\Gamma}{2s_e V} = \sum_{n=1}^{N} a_n \sin n\phi \tag{52}$$

where $\phi = \cos^{-1}\sigma$, and the loading is normal to the wing surface in the yz - plane.

The lift coefficient is given by

$$C_L = \frac{L}{qS_e} = A\int_{-1}^{1} G_z \, d\sigma = A\int_0^{\pi} G_z \sin\phi \, d\phi \tag{53}$$

where G_z is the vertical component of the loading coefficient G which itself is normal to the nonplanar wing surface. G_z is given by

$$G_z = G \cos\gamma$$

where as in equation (28)

$$\cos \gamma = [1 + (\frac{d\zeta}{d\eta})_{\phi}^{2}]^{-1/2}$$

then

$$C_L = \frac{L}{qS_e} = A\int_0^{\pi} G \cos \gamma \sin \phi \, d\phi = A \sum_{n=1}^{N} a_n \int_0^{\pi} \cos \gamma \sin\phi \quad \sin n\phi \, d\phi$$

$$= \frac{\pi A}{2} a_1 - A\sum_{n=1}^{N} a_n \int_0^{\pi} (1-\cos \gamma) \sin \phi \sin n\phi \, d\phi \qquad (54)$$

For a planar-wing winglet, γ is constant between $0 \leq \phi \leq \phi_o$, $\pi-\phi_o \leq \phi \leq \pi$ and zero between $\phi_o \leq \phi \leq \pi-\phi_o$, then equation (54) for symmetric loading reduces to

$$C_L = \frac{\pi A a_1}{2} - A(1-\cos \gamma) \left\{ a_1(\phi_o - \frac{\sin 2\phi_o}{2}) + \sum_{\substack{n=3 \\ \text{odd}}}^{N} a_n \left[\frac{\sin(n-1)\phi_o}{n-1} - \frac{\sin(n+1)\phi_o}{n+1} \right] \right\} \qquad (55)$$

Wing Bending Moment. - A wing running bending moment along the wing span coordinate σ or ϕ can be formulated for a nonplanar wing by use of the following geometry:

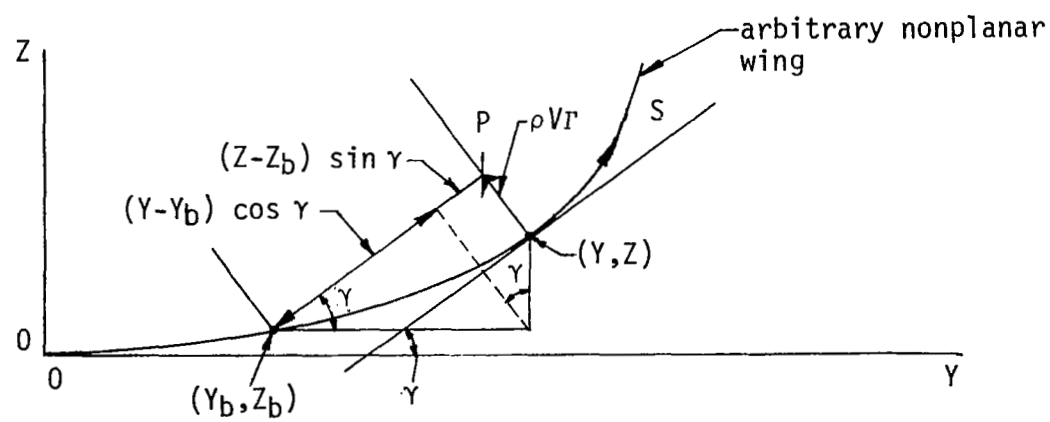

The incremental bending moment at point (y_b,z_b) is the incremental loading $\rho V\Gamma ds$ times the perpendicular moment arm between points (y_b, z_b) and P. That is

$$dM_{b_b} = \rho V\Gamma \left[(y-y_b)\cos\gamma + (z - z_b)\sin\gamma\right] ds$$

With integration and in dimensionless terms, the wing bending moment coefficient at point (η_b,ζ_b) is

$$C_{mb_b} = \frac{M_{b_b}}{qS_e 2s_e} = \frac{A}{2}\int_{\eta_b}^{1} \left[(\eta - \eta_b)\cos\gamma + (\zeta-\zeta_b)\sin\gamma\right] G\, d\sigma$$

$$= \frac{A}{2}\int_{0}^{\phi_b} \left[(\eta-\eta_b)\cos\gamma + (\zeta-\zeta_b)\sin\gamma\right] G \sin\phi d\phi$$

$$= \frac{A}{2}\sum_{n=1}^{N} a_n \int_{0}^{\phi_b} \left[(\eta-\eta_b)\cos\gamma + (\zeta-\zeta_b)\sin\gamma\right]\sin\phi \sin n\phi\, d\phi \qquad (56)$$

where G is given in equation (52) and the coordinate relations and γ are defined in equations (28) and (33).

For a planar-wing winglet the coordinate relations with $\eta_b \leq \eta_o$ are given by

$$\left.\begin{aligned} \eta-\eta_b &= \sigma-\sigma_b \\ \zeta-\zeta_b &= 0 \\ \gamma &= 0 \end{aligned}\right\} \quad 0 \leq \sigma \leq \sigma_o, \qquad \left.\begin{aligned} \eta-\eta_b &= \sigma_o-\sigma_b+(\sigma-\sigma_o)\cos\gamma \\ \zeta-\zeta_b &= (\sigma-\sigma_o)\sin\gamma \\ \gamma &= \text{constant} \end{aligned}\right\} \sigma_o \leq \sigma \leq 1 \quad (57)$$

then equation (56) simplifies to

$$C_{mb_b} = \frac{A}{2}\int_{\sigma_b}^{\sigma_o} (\sigma-\sigma_b)G d\sigma + \frac{A}{2}\int_{\sigma_o}^{1} \left[\sigma-\sigma_o + (\sigma_o-\sigma_b)\cos\gamma\right] G\, d\sigma$$

where γ is constant in the integrand. For symmetric loading with G in the Fourier series expansion, for the planar-wing winglet and $\phi_b \geq \phi_o$, this integrates into

$$C_{mb_b} = \frac{A}{8} \sum_{\substack{n=1 \\ \text{odd}}}^{N} a_n \left\{ \frac{\sin(n-2)\phi_b}{n-2} - \frac{\sin(n+2)\phi_b}{n+2} - 2\cos\phi_b \begin{bmatrix} \phi_b - \sin\phi_b\cos\phi_b, & n=1 \\ \frac{\sin(n-1)\phi_b}{n-1} - \frac{\sin(n+1)\phi_b}{n+1}, & n>1 \end{bmatrix} \right.$$

$$\left. + 2(1-\cos\gamma)(\cos\phi_b - \cos\phi_o) \begin{bmatrix} \phi_o - \sin\phi_o\cos\phi_o, & n=1 \\ \frac{\sin(n-1)\phi_o}{n-1} - \frac{\sin(n+1)\phi_o}{n+1}, & n>1 \end{bmatrix} \right\} \quad (58)$$

where C_{mb_b} is the wing bending moment coefficient at span station ϕ_b due to loading outboard of ϕ_b. The wing root bending moment is with $\phi_b = \frac{\pi}{2}$, then equation (58) reduces to

$$C_{mb_r} = \frac{A}{2} \sum_{\substack{n=1 \\ \text{odd}}}^{N} a_n \left\{ \frac{(-1)^{\frac{n+1}{2}}}{n^2-4} - \frac{1}{2}(1-\cos\gamma)\cos\phi_o \begin{bmatrix} \phi_o - \sin\phi_o\cos\phi_o, & n=1 \\ \frac{\sin(n-1)\phi_o}{n-1} - \frac{\sin(n+1)\phi_o}{n+1}, & n>1 \end{bmatrix} \right\} \quad (59)$$

The coordinate relations for running bending moment of the planar-wing winglet at points on the winglet, $\eta_b \geq \eta_o$,

$$\eta - \eta_b = (\sigma - \sigma_b)\cos\gamma$$
$$\zeta - \zeta_b = (\sigma - \sigma_b)\sin\gamma$$
$$\gamma = \text{constant}$$

then using equation (56) as before

$$C_{mb_b} = \frac{A}{2} \int_{\sigma_b}^{1} (\sigma - \sigma_b) G \, d\sigma$$

$$= \frac{A}{8} \sum_{\substack{n=1 \\ \text{odd}}}^{N} a_n \left\{ \frac{\sin(n-2)\phi_b}{n-2} - \frac{\sin(n+2)\phi_b}{n+2} - 2\cos\phi_b \begin{bmatrix} \phi_b - \sin\phi_b\cos\phi_b, & n=1 \\ \frac{\sin(n-1)\phi_b}{n-1} - \frac{\sin(n+1)\phi_b}{n+1}, & n>1 \end{bmatrix} \right\} \quad (60)$$

where the bending moment is at span station $\phi_b \leq \phi_o$, that is, ϕ_b is on the winglet.

Wing rolling moment. - Rolling moment is the same as the wing root bending moment except the spanwise loading is antisymmetric and the integration spans the wing. Thus for rolling, equation (56) becomes

$$C_l = \frac{L}{qS_e 2s_e} = \frac{A}{2}\int_0^{\pi} (\eta \cos\gamma + \zeta \sin\gamma)G \sin\phi \, d\phi \tag{61}$$

where here L denotes rolling moment and C_l is the rolling moment coefficient. For a symmetric planform and antisymmetric loading

$$C_l = A \sum_{\substack{n=2 \\ \text{even}}}^{N-1} a_n \int_0^{\pi/2} (\eta\cos\gamma + \zeta \sin\gamma) \sin\phi \sin n\phi \, d\phi \tag{62}$$

The spanwise symmetric planar-wing winglet specified in equation (57) has

$$C_l = A\int_0^{\sigma_o} \sigma G \, d\sigma + A\int_{\sigma_o}^{1} (\sigma-\sigma_o + \sigma_o \cos\gamma)G \, d\phi$$

then with antisymmetric loading

$$C_l = \frac{\pi A}{8} a_2 - \frac{A}{2}(1-\cos\gamma)\cos\phi_o \sum_{\substack{n=2 \\ \text{even}}}^{N-1} a_n \left[\frac{\sin(n-1)\phi_o}{n-1} - \frac{\sin(n+1)\phi_o}{n+1}\right] \tag{63}$$

Induced drag coefficient. - Induced drag is the spanwise integration of the product of spanwise loading normal to wing surface in the y, z plane and wake normal-to-surface induced angle. Thus

$$D_i = \rho V \int_{-s_e}^{s_e} \Gamma\alpha_i \, ds \tag{64}$$

In dimensionless terms

$$C_{D_i} = \frac{D_i}{qS_e} = A \int_{-1}^{1} G\alpha_i \, d\sigma = A \int_{0}^{\pi} G(\phi) \, \alpha_i(\phi) \sin\phi \, d\phi \tag{65}$$

With equations (52) and (50) inserted into equation (65), the drag coefficient becomes

$$C_{D_i} = \frac{\pi A}{4} \sum_{n=1}^{N} n a_n^2 + A \sum_{n=1}^{N} a_n \sum_{n^*=1}^{N} n^* a_{n^*} D_{nn^*} \tag{66}$$

$$D_{nn^*} = \int_{0}^{\pi} L_{n^*w} \sin\phi \sin n\phi \, d\phi \tag{67}$$

where L_{n^*w} is given in equations (33) and (32). This D_{nn^*} integral is of the same form as the equation (35) K_{nn^*} integral and is identical when $(2/\pi)(c/c_{av})$ equals $\sin\phi$. Comparing equations (67) and (45), it can be noticed that the D_{nn^*} coefficients have an identity with the K_{nn^*} coefficients of the elliptic wing; that is

$$D_{nn^*} = \frac{\pi^2}{8} K_{nn^*}\Big|_{\substack{\text{elliptic} \\ \text{wing}}} = \frac{\pi^2}{8} K_{nn^*}\Big|_{A \to 0} \tag{68}$$

Examination of equations (33) and (32) shows that D_{nn^*} depends only on the wing spanwise vertical displacement, the $\zeta = \zeta(\eta)$ function, and is independent of all other planform geometry such as aspect ratio, chord distribution, sweep, and wing angle variation. Thus once D_{nn^*} coefficients are tabulated for a given ζ curve, they are valid for any planform shape. For symmetric spanwise loading, L_{n^*w} is symmetric, and also only odd n and n* apply; then equations (66) and (67) simplify to

$$C_{D_i} = \frac{\pi A}{4} \sum_{\substack{n=1 \\ \text{odd}}}^{N} n \, a_n^2 + A \sum_{\substack{n=1 \\ \text{odd}}}^{N} a_n \sum_{\substack{n^*=1 \\ \text{odd}}}^{N} n^* a_{n^*} D_{nn^*} \tag{69}$$

$$D_{nn^*} = 2\int_0^{\pi/2} L_{n^*w} \sin\phi \sin n\phi \, d\phi, \text{ for odd } n \text{ and } n^* \tag{70}$$

The D_{nn^*} coefficients of the planar-wing winglet configuration with symmetric spanwise loading are determined in the same manner as done for the K_{nn^*} coefficients of equation (40). After employing this similarity relation, which is simply the substitution of sin ϕ_w for $(2/\pi)(c/c_{av})$ into equation (40), equation (70) becomes

$$D_{nn^*} = \frac{\pi}{M+1}\left(L_{n^*\frac{M+1}{2}} \sin n\frac{\pi}{2} + 2\sum_{w=1}^{\frac{M-1}{2}} L_{n^*w} \sin\phi_w \sin n\phi_w\right) \tag{71}$$

where $\phi_w = w\pi/(M+1)$, and M, n, and n* are odd integers. For the planar-wing winglet L_{n^*w}'s are determined from the appropriate ϕ_w range of equations (21) or (22) (in which n is changed to n*).

Example computations have been made for one planar-wing winglet configuration; that is, for $\phi_o = 5\pi/32$ radian or $\sigma_o = .8819$ which is the span station at which the winglet begins. For M = 15, then $\phi_w = w\pi/16$, the L_{n^*w} computed from equations (21) and (22) are presented in table I. With these L_{n^*w} values, the D_{nn^*} coefficients are determined from equation (71) using M = 15. D_{nn^*} coefficients are presented in table II. When these D_{nn^*} values are inserted into equation (69), the induced drag coefficient depends only on the spanwise circulation distribution or laterally surface spanwise loading distribution normal to the surface, and is independent of planform shape including winglet shape or sweep. This planform is nonplanar and is for a planar-wing winglet with wing tip winglets starting at $\sigma_o = .8819$ span station with winglet at a given γ angle.

PLANAR-WING WINGLET LOADING SOLUTION

FOR RECTANGULAR WING

The sample application of the theory developed in the previous chapter demonstrates the usage of the method. The example wing configuration is a symmetric wing with winglet at each wing tip, the combination being described as a planar-wing winglet. Particularly, the rectangular wing and the slender wing is investigated in detail. An objective is to show example solutions of equations (39) and (49) for the prediction of a_n/a_1 Fourier loading coefficients.

Chord Distribution for Tapered Planar-Wing Winglet

The chord distribution is

$$\begin{aligned} c &= c_r - (c_r - c_o)\frac{\sigma}{\sigma_o}, \quad 0 \le \sigma \le \sigma_o \\ &= c_{wo} - (c_{wo} - c_{wt})\left(\frac{\sigma-\sigma_s}{1-\sigma_o}\right), \quad \sigma_o \le \sigma \le 1 \end{aligned} \tag{72}$$

where c_r is wing root chord, c_o is wing chord at span station σ_o, c_{wo} is winglet chord at span station σ_o, and c_{wt} is winglet chord at winglet tip ($\sigma = 1$). The chord distribution of equation (72) leads to the following wing geometry relations

$$S_e = c_r s_e[(1+\lambda_o)\sigma_o + \lambda_{wo}(1+\lambda_w)(1-\sigma_o)], \quad A = \frac{4s_e^2}{S_e}, \quad c_{av} = \frac{S_e}{2s_e} \tag{73}$$

$$\frac{c_r}{c_{av}} = \frac{2}{(1+\lambda_o)\sigma_o + \lambda_{wo}(1+\lambda_w)(1-\sigma_o)} \tag{74}$$

$$\begin{aligned} \frac{c}{c_{av}} &= \frac{c_r}{c_{av}}\left(1 - \frac{1-\lambda_o}{\sigma_o}\sigma\right), \quad 0 < \sigma < \sigma_o \\ &= \frac{c_r}{c_{av}}\lambda_{wo}\left(1 + \frac{1-\lambda_w}{1-\sigma_o}\sigma_o - \frac{1-\lambda_w}{1-\sigma_o}\sigma\right), \sigma_o \le \sigma \le 1 \end{aligned} \tag{75}$$

where $\lambda_o = c_o/c_r$ is planar-wing taper ratio, $\lambda_w = c_{wt}/c_{wo}$ is winglet taper ratio, and $\lambda_{wo} = c_{wo}/c_r$ is ratio of winglet root chord to wing root chord, and $\sigma = \cos\phi$, $\sigma_o = \cos\phi_o$.

Planform Fourier Coefficients

From equation (35), the c_p coefficients are obtained from the integration

$$c_p = \frac{2}{\pi}\int_0^{\pi} \frac{c}{c_{av}} \sin p\phi \, d\phi \overset{p=1}{=} \frac{4}{\pi} \tag{76}$$

where, for the tapered planar-wing winglet, c/c_{av} is given by equation (75). For a rectangular wing with rectangular winglet, equations (74) and (75) reduce to

$$\frac{c}{c_{av}} = \frac{1}{\lambda_{wo}+(1-\lambda_{wo})\cos\phi_o}, \quad \phi_o \le \phi \le \frac{\pi}{2}$$

$$= \frac{\lambda_{wo}}{\lambda_{wo}+(1-\lambda_{wo})\cos\phi_o}, \quad 0 \le \phi \le \phi_o \tag{77}$$

where $\lambda_{wo} = c_{winglet}/c_{wing}$, and c/c_{av} is symmetric with respect to ϕ. Inserting equation (77) into equation (76) the c_p coefficients are

$$c_p = \frac{4}{\pi p}\frac{\lambda_{wo}+(1-\lambda_{wo})\cos p\phi_o}{\lambda_{wo}+(1-\lambda_{wo})\cos\phi_o}, \text{ odd p only} \tag{78}$$

From equation (35) the I_{nn*} coefficients are given by

$$I_{nn*} = \sum_{\substack{p=|n-n*|-1 \\ \text{odd}}}^{n+n*-1} c_p \tag{79}$$

The α_c distribution of equation (28), for the planar-wing winglet is given by

$$\begin{aligned} \alpha_c &= \alpha+\varepsilon \ , \quad \phi_o \le \phi \le \frac{\pi}{2} \\ &= \alpha\cos\gamma + \varepsilon + \psi, \quad 0 \le \phi \le \phi_o \end{aligned} \tag{80}$$

where α is independent of ϕ; however, ε and ψ can be functions of ϕ. Assuming only additional loading conditions, then twist ε is zero, and assume that the toe in angle ψ is constant along the winglet. Then the $c_{\alpha n}$ coefficient of equation (35) with equations (77) and (80), becomes

$$c_{\alpha n} = \frac{4\alpha}{\pi n} \frac{\lambda_{wo}\left(\cos\gamma + \frac{\psi}{\alpha}\right) + \left[1 - \lambda_{wo}\left(\cos\gamma + \frac{\psi}{\alpha}\right)\right] \cos n\,\phi_o}{\lambda_{wo} + (1 - \lambda_{wo})\cos\phi_o}, \text{ odd n only} \tag{81}$$

which is the $c_{\alpha n}$ for an untwisted rectangular wing with rectangular winglet of chord $c_{winglet} = \lambda_{wo}\, c_{wing}$, with winglet extending from span station $\phi = 0$ to ϕ_o, at constant dihedral cant angle γ from the wing plane, with toein angle ψ.

Nonplanar K_{nn}* Coefficients

For the planar-wing winglet, these coefficients are obtained from equation (41). The $L_{n}{}^{*}{}_{w}$ coefficients in this equation are independent of chord distribution, hence, once known for a given ϕ_o and γ, they can be combined with any chord distribution for evaluating K_{nn}* coefficients. Example values of $L_{n}{}^{*}{}_{w}$ for $\phi_o = 5\pi/32$ radians and $\gamma = 90$ and 75 degrees are shown in table I. These values are based on computations with M = 15 and with $\phi_w = w\pi/16$. For an M = 15 computation these $L_{n}{}^{*}{}_{w}$ can be inserted into equation (41) and K_{nn}* computed with (c/c_{av}) given by equations (75) or (77) in which, $\sigma = \cos\phi_w = \cos(w\pi/16)$ and $\sigma_o = \cos(5\pi/32) = .88192$. Example values of K_{nn}* are presented in table III for a rectangular wing with rectangular winglet with $c_{winglet} = c_{wing}$; that is, $\lambda_{wo} = 1$.

Loading Solution for Rectangular Wing with $\lambda_{wo} = 1$ Winglet

This wing-winglet has the geometry

$$S_e = 2\,c\,s_e,\quad A = \frac{2\,s_e}{c},\quad \frac{c}{c_{av}} = 1 \tag{82}$$

then, from equation (78)

$$c_p = \frac{4}{\pi p},\quad c_n = \frac{4}{\pi n},\quad c_{n^*} = \frac{4}{\pi n^*},\quad \text{odd } p,\ n,\ n^* \text{ only} \tag{83}$$

Equation (79) becomes

$$\frac{\pi}{4} I_{nn^*} = \sum_{\substack{p = |n-n^*| \\ \text{odd}}}^{n+n^*-1} \frac{1}{p} - 1 \tag{84}$$

and equation (81) reduces to

$$c_{\alpha n} = \frac{4\alpha}{\pi n}\left[\cos\gamma + \frac{\psi}{\alpha} + \left(1 - \cos\gamma - \frac{\psi}{\alpha}\right)\cos n\phi_o\right],\quad \text{odd } n \text{ only} \tag{85}$$

Equations (38) and (39) become

$$a_1 = \frac{4\left[\cos\gamma + \frac{\psi}{\alpha} + \left(1-\cos\gamma - \frac{\psi}{\alpha}\right)\cos\phi_o\right]}{A + 2k\left[1 + \frac{\pi}{2}K_{11} + \sum_{\substack{n^*=3 \\ \text{odd}}}^{N}\left(1+\frac{\pi}{2}n^*K_{1n^*}\right)\frac{a_{n^*}}{a_1}\right]} \tag{86}$$

$$\frac{a_n}{a_1} = \frac{c_{\alpha n}}{c_{\alpha 1}}\left[1+\frac{2k}{A}\left(1+\frac{\pi}{2}K_{11}\right)\right] - \frac{2k}{A}\left(\frac{1}{n} + \frac{\pi}{2}K_{n1}\right) + \frac{2k}{A}\sum_{\substack{n^*=3 \\ \text{odd}}}^{N}\left[\frac{c_{\alpha n}}{c_{\alpha 1}}\left(1+n^*\frac{\pi}{2}K_{1n^*}\right) - n^*\frac{\pi}{4}I_{nn^*} - n^*\frac{\pi}{2}K_{nn^*}\right]\frac{a_{n^*}}{a_1} \tag{87}$$

for $n = 3, 5, 7, \ldots N$

where

$$\frac{c_{\alpha n}}{c_{\alpha 1}} = \frac{1}{n} \frac{\cos\gamma + \frac{\psi}{\alpha} + (1 - \cos\gamma - \frac{\psi}{\alpha})\cos n\phi_o}{\cos\gamma + \frac{\psi}{\alpha} + (1 - \cos\gamma - \frac{\psi}{\alpha})\cos\phi_o} \tag{88}$$

and $n^*(\pi/4)\ I_{nn^*}$ values determined from equation (84) are tabulated in table IV.

Slender Wing Theory

As aspect ratio becomes small, the planform becomes slender and independent of wing or winglet planform shape or sweep if trailing edge cutout is behind leading edge. With the $\varepsilon = 0$, α_c distribution of equation (80) inserted into the $c_{\alpha n}$ integral of equation (45), the $c_{\alpha n}$ for $A \to 0$ is

$$\left.\begin{aligned} c_{\alpha 1} &= \frac{8\alpha}{\pi^2}\left[\frac{\pi}{2} - (1 - \cos\gamma - \frac{\psi}{\alpha})(\phi_o - \sin\phi_o\cos\phi_o)\right] \\ c_{\alpha n} &= \frac{-8\pi}{\pi^2}(1 - \cos\gamma - \frac{\psi}{\alpha})\left[\frac{\sin(n-1)\phi_o}{n-1} - \frac{\sin(n+1)\phi_o}{n+1}\right],\ \text{odd } n > 1 \end{aligned}\right\} \tag{89}$$

then the ratio is

$$\frac{c_{\alpha n}}{c_{\alpha 1}} = -\frac{(1 - \cos\gamma - \frac{\psi}{\alpha})\left[\frac{\sin(n-1)\phi_o}{n-1} - \frac{\sin(n+1)\phi_o}{n+1}\right]}{\frac{\pi}{2} - (1 - \cos\gamma - \frac{\psi}{\alpha})(\phi_o - \sin\phi_o\cos\phi_o)},\ \text{odd } n > 1 \tag{90}$$

Comparing the equation (45) K_{nn^*} coefficients for slender wings with the D_{nn^*} drag parameter coefficients of equation (67) it can be seen that

$$K_{nn^*}{}_{A \to 0} = \frac{8}{\pi^2} D_{nn^*} \tag{91}$$

With equation (91), the slender wing equations (49) for determining symmetric loading Fourier coefficients become

$$a_1 = \frac{\pi c_{\alpha 1}}{4\left(1 + \frac{4}{\pi}D_{11} + \sum_{\substack{n^*=3 \\ \text{odd}}}^{N} n^*\frac{4}{\pi}D_{1n^*}\frac{a_{n^*}}{a_1}\right)} \tag{92}$$

$$\frac{a_n}{a_1} = \frac{1}{n}\frac{c_{\alpha n}}{c_{\alpha 1}} + \frac{1}{n}\left(\frac{c_{\alpha n}}{c_{\alpha 1}}\frac{4}{\pi}D_{11} - \frac{4}{\pi}D_{n1}\right) + \frac{1}{n}\sum_{\substack{n^*=3 \\ \text{odd}}}^{N}\left(\frac{c_{\alpha n}}{c_{\alpha 1}}n^*\frac{4}{\pi}D_{1n^*} - n^*\frac{4}{\pi}D_{nn^*}\right)\frac{a_{n^*}}{a_1} \qquad (93)$$

for $n = 3, 5, \ldots N$

where $c_{\alpha n}$ is from equation (45), with α_c from equation (28), and D_{nn^*} from equation (67). Equations (92) and (93) are general for obtaining nonplanar slender wing solutions. The first term in equation (93) (that is, with $D_{nn^*} = 0$) is the slender wing planar wing solution derived in reference 8. For the planar-wing winglet configuration, the $c_{\alpha n}$ values are those in equations (89) and (90), and D_{nn^*} coefficients are determined from equation (71).

a_n Coefficients for Aspect Ratio Approaching Infinity

These a_n coefficients are given in equation (47) and are directly in terms of $c_{\alpha n}$. Thus as $A \to \infty$

$$a_1 \to \frac{\pi c_{\alpha 1}}{A}, \quad \frac{a_n}{a_1} \to \frac{c_{\alpha n}}{c_{\alpha 1}} \qquad (94)$$

where with $c_{\alpha n}$ values of equation (81), the a_n values for a rectangular wing with rectangular winglet for $A \to \infty$ are

$$\left.\begin{aligned} a_1 &\to \frac{4\alpha}{A}\,\frac{\lambda_{wo}\left(\cos\gamma + \frac{\psi}{\alpha}\right) + \left[1 - \lambda_{wo}\left(\cos\gamma + \frac{\psi}{\alpha}\right)\right]\cos\phi_o}{\lambda_{wo} + (1 - \lambda_{wo})\cos\phi_o} \\ \frac{a_n}{a_1} &\to \frac{1}{n}\,\frac{1 + \left[\lambda_{wo}^{-1}\left(\cos\gamma + \frac{\psi}{\alpha}\right)^{-1} - 1\right]\cos n\phi_o}{1 + \left[\lambda_{wo}^{-1}\left(\cos\gamma + \frac{\psi}{\alpha}\right)^{-1} - 1\right]\cos\phi_o} \end{aligned}\right\} \qquad (95)$$

With $\lambda_{wo} = 1$, equation (95) simplifies to,

$$a_1 \to \frac{4\alpha}{A}\left[\cos\phi_o + (1 - \cos\phi_o)\left(\cos\gamma + \frac{\psi}{\alpha}\right)\right]$$

$$\frac{a_n}{a_1} \to \frac{1}{n}\,\frac{1 + \left[\left(\cos\gamma + \frac{\psi}{\alpha}\right)^{-1} - 1\right]\cos n\,\phi_o}{1 + \left[\left(\cos\gamma + \frac{\psi}{\alpha}\right)^{-1} - 1\right]\cos\phi_o} \qquad (96)$$

which is for a rectangular wing with rectangular winglet having the same chord as the wing.

Rectangular Wing Winglet Numerical Solutions for a_n and Force and Moment Coefficients

These example solutions are all for rectangular wing and rectangular winglet with winglet chord equal to wing chord. However, as aspect ratio becomes small these data apply to arbitrary wing and winglet shape as born out by the slender wing theory. Parameter values that remain the same in this numerical example include

$$\lambda_o = \lambda_w = \lambda_{wo} = 1, \quad \phi_o = 5\pi/32 \text{ rad}, \quad \sigma_o = \cos\phi_o = .88192, \quad M = 15, \quad N = 9 \qquad (97)$$

Parameters which have various values include

$$A, \ \gamma, \ \psi \qquad (98)$$

With N = 9 equation (87) becomes four linear simultaneous equations in a_n/a_1. From equation (24) $k = (A + 3.79)/(A + 1.895)$. Also define ψ_n as a shortened notation for equation (88) which with γ = 90 degrees and ϕ_o = 5 /32 radians = 28.125 degrees results in

$$\psi_n = \frac{c\alpha_n}{c_{\alpha 1}} = \frac{1}{n}\,\frac{\frac{\psi}{\alpha} + (1 - \frac{\psi}{\alpha})\cos(28.125\ n)}{.88192 + .11808\,\frac{\psi}{\alpha}} \qquad (99)$$

Then with I_{nn*} values from table IV and the γ = 90 degrees values of K_{nn*} from table III the four linear equations become

$$\left(\frac{A}{k} + 2.0702\right)\psi_3 - .69737 = \left(\frac{A}{k} + 8.5589 - 1.8682\ \psi_3\right)\frac{a_3}{a_1} + (6.5716 - 1.9083\ \psi_3)\frac{a_5}{a_1}$$
$$+ (6.3840 - 2.0005\ \psi_3)\frac{a_7}{a_1} + (6.2065 - 1.8933\ \psi_3)\frac{a_9}{a_1}$$

$$\left(\frac{A}{k} + 2.0702\right)\psi_5 - .44574 = (3.4571 - 1.8682\ \psi_5)\frac{a_3}{a_1} + \left(\frac{A}{k} + 17.6827 - 1.9083\psi_5\right)\frac{a_5}{a_1}$$
$$+ (12.7130 - 2.0005\psi_5)\frac{a_7}{a_1} + (11.5070 - 1.8933\ \psi_5)\frac{a_9}{a_1} \qquad (100)$$

$$\left(\frac{A}{k} + 2.0702\right)\psi_7 - .40765 = (2.6664 - 1.8682\ \psi_7)\frac{a_3}{a_1} + (9.2030 - 1.9088\ \psi_7)\frac{a_5}{a_1}$$
$$+ \left(\frac{A}{k} + 28.0203 - 2.0005\ \psi_7\right)\frac{a_7}{a_1} + (18.6383 - 1.8933\psi_7)\frac{a_9}{a_1}$$

$$\left(\frac{A}{k} + 2.0702\right)\psi_9 - .30123 = (2.3797 - 1.8682\ \psi_9)\frac{a_3}{a_1} + (6.8409 - 1.9088\ \psi_9)\frac{a_5}{a_1}$$
$$+ (14.5977 - 2.0005\ \psi_9)\frac{a_7}{a_1} + \left(\frac{A}{k} + 37.2048 - 1.8933\psi_9\right)\frac{a_9}{a_1}$$

When A and ψ/α are specified, a simultaneous solution of these four gives the a_n/a_1 from n = 3 through 9. With a_n/a_1 known, a_1/α can be evaluated from equation (86) which, with γ = 90 degrees and $\phi_o = 5\pi/32$, becomes

$$\frac{a_1}{\alpha} = \frac{3.5277\ (1 + .13389\ \frac{\psi}{\alpha})}{A + 2k\ (1.0351 + .9341\ \frac{a_3}{a_1} + .9542\ \frac{a_5}{a_1} + \frac{a_7}{a_1} + .9467\ \frac{a_9}{a_1})} \qquad (101)$$

Loading equations for other γ angles using equations (86), (87), and (88) can be written in a similar manner to those of equations (100) and (101). It can be noted that with $\gamma = 0$, $K_{nn}^* = 0$, which is a plannar wing-winglet configuration. Values of a_n determined from equations (100) and (101) and for other γ angles are presented in table V.

Slender wing. - With $A \to 0$, solutions of equations (93) and (92) are needed. For ϕ_o = 28.125 degrees, equation (90) becomes

$$\frac{c_{\alpha n}}{c_{\alpha 1}} = \frac{-.6686\ (1 - \cos\gamma - \frac{\psi}{\alpha})}{1 + .05024\ (\cos\gamma + \frac{\psi}{\alpha})} \left[\frac{\sin\ (n-1)\ 28.125}{n-1} - \frac{\sin\ (n+1)\ 28.125}{n+1}\right] \quad (102)$$

where the value within the brackets for n = 3, 5, 7, . . . odd is respectively, .18477, .19846, .12090, .00969, -.09870, -.07157, -.02282, .03164, and so on. The coefficient $c_{\alpha 1}$ is determined from equation (89) which, for $\phi_0 = 28.125$ becomes

$$\frac{c_{\alpha 1}}{\alpha} = 1.212334\ [1 + .05024\ (\cos\gamma + \frac{\psi}{\alpha})] \quad (103)$$

then, from equation (92), the a_1/α coefficient for $A \to 0$, $\phi_0 = 5\pi/32$ radians, and N = 9, is

$$\frac{a_1}{\alpha} = \frac{.95217\ [1 + .05024\ (\cos\gamma + \frac{\psi}{\alpha})]}{1 + \frac{4}{\pi} D_{11} + \sum_{\substack{n^*=3 \\ \text{odd}}}^{9} n^* \frac{4}{\pi} D_{1n^*} \frac{a_{n^*}}{a_1}} \quad (104)$$

For an $A \to 0$, N = 9 solution for a_n's, equation (93) is solved. The value of $c_{\alpha n}/c_{\alpha 1}$ is given in equation (102) and $n^*(4/\pi)D_{nn^*}$ values are in table II. With $\gamma = 90°$ equation (93) is

$$\begin{aligned}
-.00111 + .04255\ \psi_0 &= (-.94063 - .00027\ \psi_0)\frac{a_3}{a_1} + (.05642 + .00007\ \psi_0)\frac{a_5}{a_1} \\
&\quad + (.01882 + .00051\ \psi_0)\frac{a_7}{a_1} + (.00965 + .00255\ \psi_0)\frac{a_9}{a_1} \\
-.00052 + .02742\ \psi_0 &= (.03267 - .00018\ \psi_0)\frac{a_3}{a_1} + (-.98172 + .00004\ \psi_0)\frac{a_5}{a_1} \\
&\quad + (-.00323 + .00033\ \psi_0)\frac{a_7}{a_1} + (-.02269 + .00033\ \psi_0)\frac{a_9}{a_1} \quad (105) \\
.00519 + .01193\ \psi_0 &= (-.00349 - .00008\ \psi_0)\frac{a_3}{a_1} + (-.01700 + .00002\ \psi_0)\frac{a_5}{a_1} \\
&\quad + (-1.02633 + .00014\ \psi_0)\frac{a_7}{a_1} + (-.01645 + .00072\ \psi_0)\frac{a_9}{a_1} \\
.00351 + .00074\ \psi_0 &= -.01391\frac{a_3}{a_1} - .01908\frac{a_5}{a_1} + (-.00932 + .00001\ \psi_0)\frac{a_7}{a_1} \\
&\quad + (-.99630 + .00004\ \psi_0)\frac{a_9}{a_1}
\end{aligned}$$

where

$$\psi_0 = \frac{1 - \frac{\psi}{\alpha}}{1 + .05024 \frac{\psi}{\alpha}} \tag{106}$$

With γ = 90 degrees, equation (104) reduces to

$$\frac{a_1}{\alpha} = \frac{.92144 \left(1 + .05024 \frac{\psi}{\alpha}\right)}{1 + .00645 \frac{a_3}{a_1} - .00162 \frac{a_5}{a_1} - .01203 \frac{a_7}{a_1} - .05992 \frac{a_9}{a_1}} \tag{107}$$

When ψ/α is specified, a simultaneous solution of the equations of equation (105) evaluates a_n/a_1 from n = 3 through 9. The first Fourier loading coefficient is given in equation (107). $A \to 0$ loading equations for other γ angles are obtained similarly to the γ = 90 degrees example. Values of a_n, determined for $A \to 0$ from equations (105) and (107), and for other γ angles are presented in table V.

With slender wing nonplanar theory a reasonable approximation for a_n/a as seen by examining equation (93) is, since D_{nn^*} values are not large

$$\frac{a_n}{a_1} \simeq \frac{1}{n} \frac{c_{\alpha n}}{c_{\alpha 1}} \tag{108}$$

where $c_{\alpha n}/a_1$ for $A \to 0$ are given in equation (102). A better approximation is to use equation (108) for approximating a_{n^*}/a_1 under the summation sign. Then

$$\frac{a_n}{a_1} \simeq \frac{\frac{c_{\alpha n}}{c_{\alpha 1}} \left(1 + \frac{4}{\pi} D_{11}\right) - \frac{4}{\pi} D_{n1} + \frac{4}{\pi} \sum_{\substack{n^*=3 \\ \text{odd}}}^{N}{}' \left(\frac{c_{\alpha n}}{c_{\alpha 1}} D_{1n^*} - D_{nn^*}\right) \frac{c_{\alpha n^*}}{c_{\alpha 1}}}{n \left(1 + \frac{4}{\pi} \frac{c_{\alpha n}}{c_{\alpha 1}} D_{1n} - \frac{4}{\pi} D_{nn}\right)} \tag{109}$$

where the prime on the summation sign means the term is not summed when $n^* = n$. The coefficients D_{1n} and D_{nn} symbolize D_{1n^*} and D_{nn^*} for $n^* = n$. In this form a_n/a_1 can be determined directly and does not involve a simultaneous equations solution. When a_n/a_1 are known, a_1 is computed from the equation (92) relation.

$A \to \infty$ solution. - With $\phi_0 = 28.125$ degrees equation (96) becomes

$$\frac{a_1}{\alpha} \to \frac{3.5277}{A}\left[1 + .1339\left(\cos\gamma + \frac{\psi}{\alpha}\right)\right] \tag{110}$$

$$\frac{a_n}{a_1} \to \frac{1.1339}{n}\,\frac{\cos\gamma + \frac{\psi}{\alpha} + \left(1 - \cos\gamma - \frac{\psi}{\alpha}\right)\cos(28.125\,n)}{1 + .1339\left(\cos\gamma + \frac{\psi}{\alpha}\right)} \tag{111}$$

Equations (110) and (111) are the a_n coefficients for a rectangular wing winglet with winglet chord equal to wing chord, as aspect ratio approaches infinity. Example numerical values are included in the data of table V.

Lift coefficient. - With $\phi_0 = 28.125$ degrees, N = 9, equation (55) becomes

$$C_{L_\alpha} = \frac{\pi A a_1}{2\alpha}\left[1 - (1-\cos\gamma)\left(.047835 + .11763\,\frac{a_3}{a_1} + .12634\,\frac{a_5}{a_1} + .07697\,\frac{a_7}{a_1} + .00617\,\frac{a_9}{a_1}\right)\right] \tag{112}$$

Using equation (112) with the a_n in table V, the lift-curve slope of the various wing-winglet configurations can be evaluated, and these are presented in table V.

Root bending moment coefficient. - With $\phi_0 = 28.125$ degrees, N = 9, equation (59) becomes

$$\frac{C_{m_{b_r}}}{\alpha} = \frac{A\,a_1}{6\alpha}\left[1 + \frac{3}{5}\frac{a_3}{a_1} - \frac{1}{7}\frac{a_5}{a_1} + \frac{1}{15}\frac{a_7}{a_1} - \frac{3}{77}\frac{a_9}{a_1} - (1-\cos\gamma)\left(.099400 + .24443\,\frac{a_3}{a_1} + .26254\,\frac{a_5}{a_1} + .15994\,\frac{a_7}{a_1} + .01282\,\frac{a_9}{a_1}\right)\right] \tag{113}$$

Using equation (113) with the a_n in table V, the wing root bending moment coefficient of the various wing-winglet configurations can be evaluated and these are presented in table V.

Induced drag coefficient. - With N = 9, equation (69) becomes

$$\frac{C_{D_i}}{\alpha^2} = \frac{\pi A}{4}\left(\frac{a_1}{\alpha}\right)^2 \left[\sum_{\substack{n=1 \\ \text{odd}}}^{9} n \left(\frac{a_n}{a_1}\right)^2 + \sum_{\substack{n=1 \\ \text{odd}}}^{9} \frac{a_n}{a_1} \sum_{\substack{n^*=1 \\ \text{odd}}}^{9} \frac{a_{n^*}}{a_1} n^* \frac{4}{\pi} D_{nn^*} \right] \tag{114}$$

where, with ϕ_o = 28.125 degrees and γ angles of 90 and 75 degrees, $n^*(4/\pi)\ D_{nn^*}$ are listed in table II. Then, with γ = 90 degrees, equation (114) leads to

$$\begin{aligned}\frac{C_{D_i}}{\pi A \alpha^2} = \frac{1}{4}\left(\frac{a_1}{\alpha}\right)^2 \Bigg[& 1.03335 + \frac{a_3}{a_1}\left(.00333 + 2.82191\,\frac{a_3}{a_1} - .33261\,\frac{a_5}{a_1} - .03205\,\frac{a_7}{a_1}\right. \\ & \left. + .09628\,\frac{a_9}{a_1}\right) + \frac{a_5}{a_1}\left(-.00425 + 4.90862\,\frac{a_5}{a_1} + .19985\,\frac{a_7}{a_1} + .28517\,\frac{a_9}{a_1}\right) \\ & + \frac{a_7}{a_1}\left(.02387 + 7.18434\,\frac{a_7}{a_1} + .19903\,\frac{a_9}{a_1}\right) + \frac{a_9}{a_1}\left(-.03036 + 8.96666\,\frac{a_9}{a_1}\right) \Bigg]\end{aligned} \tag{115}$$

An induced drag expression similar to that of equation (115) can be made for the γ = 75 degrees configuration by using the D_{nn^*} coefficients of table II with γ = 75°. Induced drag coefficients computed from equations (114) and (115) are presented in table V.

The drag efficiency factor e is

$$e = \frac{C_L{}^2}{\pi A C_{D_i}} = \frac{(C_{L_\alpha}/\pi A)^2}{C_{D_i}/\pi A \alpha^2} \tag{116}$$

This drag factor e is given in table V as determined from the lift and drag coefficient parameters listed in that table.

Ratio of Induced Drag of Planar-Wing Winglet to that of Flat Planar Wing with Equal Lift and Root Bending Moment

A measure of the efficiency of a wing-winglet configuration is to compare the configuration with a flat planar wing with the same lift and root bending moment as that of the wing-winglet. The efficiency is measured in

terms of induced drag. Let subscript p denote a flat planar wing. Then the induced drag is

$$D_{ip} = \frac{L_p^2}{\pi q b_p^2 e_p}, \quad D_i = \frac{L^2}{4\pi q s_e^2 e}$$

where the second equation is the induced drag of the wing-winglet configuration. In ratio form

$$\frac{D_i}{D_{ip}} = \left(\frac{L}{L_p}\right)^2 \left(\frac{b_p}{2s_e}\right)^2 \frac{e_p}{e} \tag{117}$$

The ratio of root bending moment coefficients gives

$$\frac{C_{mb_r}/C_L}{(C_{mb_r}/C_L)_p} = \frac{M_{b_r}/2Ls_e}{M_{b_{rp}}/Lb_p} = \frac{M_{b_r}}{M_{b_{rp}}} \frac{L_p}{L} \frac{b_p}{2s_e} \tag{118}$$

For the flat planar wing

$$\left(\frac{C_{mb_r}}{C_L}\right)_p = \frac{1}{4} \frac{y_{cp}}{b/2} = \frac{1}{4} \eta_{cp} \tag{119}$$

where η_{cp} is the spanwise center of pressure along the semispan. For the condition of equal lift and equal bending moment, $b_p/2s_e$, according to equation (118), must be

$$\frac{b_p}{2s_e} = \frac{4}{\eta_{cp}} \frac{C_{mb_r}}{C_L} \tag{120}$$

and the drag ratio from equation (118) becomes

$$\frac{D_i}{D_{ip}} = \left(\frac{4}{\eta_{cp}} \frac{C_{mb_r}}{C_L}\right)^2 \frac{e_p}{e} \tag{121}$$

The ratio of aspect ratio of the flat planar wing to that of the wing-winglet is

$$\frac{A_p}{A} = \left(\frac{b_p}{2s_e}\right)^2 \frac{S_e}{S_p} \tag{122}$$

When surface areas are the same, friction drag will remain about equal. With the condition $S_p = S_e$

$$\frac{A_p}{A} = \left(\frac{b_p}{2s_e}\right)^2 = \left(\frac{4}{\eta_{cp}} \frac{C_{mb_r}}{C_L}\right)^2 \tag{123}$$

then the drag ratio is

$$\frac{D_i}{D_{i_p}} = \frac{A_p}{A} \frac{e_p}{e} \tag{124}$$

Flat planar elliptic wing. - Since the elliptic wing is the most efficient in terms of drag, it serves as a good standard for comparison with nonplanar wings. Also the elliptic wing is analytically the simplest. For the elliptic wing

$$\eta_{cp} = \frac{4}{3\pi} \text{ , } e_p = 1 \tag{125}$$

then from equations (123) and (124)

$$\frac{A_p}{A} = \left(3\pi \frac{C_{mb_r}}{C_L}\right)^2 \text{ , } \frac{D_i}{D_{i_p}} = \frac{A_p}{A} \frac{1}{e} \tag{126}$$

Values of these ratios have been computed using the data of table V. Results are shown in table VI.

Flat planar rectangular wing. - Another standard for comparison is to compare the nonplanar wing with a flat planar wing having the same chord distribution. In the present problem, the nonplanar wing-winglet has a rectangular shape. For flat planar rectangular wings, it is convenient to use

$$e_p = \frac{1}{1 + \delta} \tag{127}$$

$$C_{L_{\alpha p}} = \frac{2\pi A_p}{A_p + 2k_p(1 + \tau)} \tag{128}$$

where, from equation (286) of reference 6

$$\delta = .01453 \log_e \left[1 + (.52 \frac{A}{k})^2 + (.26848 \frac{A}{k})^6 + (.07 \frac{A}{k})^{14}\right]_p \tag{129}$$

$$\tau = .10467 \log_e \left[1 + .385 \frac{A}{k} + (.19167 \frac{A}{k})^2\right]_p \tag{130}$$

where the subscript p indicates that the A and k are for the flat planar rectangular wing. The value of $k_p = (A_p + 3.79)/(A_p + 1.895)$ is given in equation (24). Based on the analytical data of the rectangular wing (ref. 6), the spanwise center of pressure can be formulated as

$$\eta_{cp} = \frac{1}{2} - \frac{1.5573}{(\frac{A}{k} + A + 20.6)_p} \tag{131}$$

In a squared formulation

$$\eta_{cp}^2 \simeq \frac{.25\ A_p + 2.183}{A_p + 12.121} \tag{132}$$

Inserting this η_{cp} in equation (123) leads to a quadratic equation in A_p. Thus

$$\frac{A_p}{A} = 16\ (\frac{C_{mb_r}}{C_L})^2\ \frac{A_p + 12.121}{.25\ A_p + 2.183}$$

hence

$$A_p^2 + \left[8.732 - 64(\frac{C_{mb_r}}{C_L})^2 A\right] A_p - 775.744\ (\frac{C_{mb_r}}{C_L})^2\ A = 0 \tag{133}$$

Thus, with a computed nonplanar wing value of C_{mb_r}/C_L for a given aspect ratio A, the equivalent planar wing A_p is obtained by solving the quadratic equation (133). With A_p known, e_p is determined from equations (127) and (129). Then the drag ratio is determined from equation (124). Values of these drag ratios have been computed using the data of table V with results shown in table VI.

$A \to \infty$. - As aspect ratio approaches infinity the wing circulation becomes directly

$$\frac{2\Gamma}{cV} = 2\pi\alpha_c \tag{134}$$

then similarly to the formulation of equation (54) and (56)

$$C_{L_\alpha} = 2\pi \int_0^1 \frac{\alpha_c}{\alpha} \frac{c}{c_{av}} \cos\gamma \, d\sigma \tag{135}$$

$$\frac{C_{mb_r}}{\alpha} = \pi \int_0^1 \frac{\alpha_c}{\alpha} \frac{c}{c_{av}} (\eta \cos\gamma + \zeta \sin\gamma) \, d\sigma \tag{136}$$

For the planar-wing winglet, these equations become

$$C_{L_\alpha} = 2\pi \left[\int_0^{\sigma_o} \frac{c}{c_{av}} \, d\sigma + (\cos\gamma + \frac{\psi}{\alpha})\cos\gamma \int_{\sigma_o}^1 \frac{c}{c_{av}} \, d\sigma \right] \tag{137}$$

$$\frac{C_{mb_r}}{\alpha} = \frac{\pi}{2} \int_0^{\sigma_o} \frac{c}{c_{av}} \, \sigma d\sigma + \frac{\pi}{2} (\cos\gamma + \frac{\psi}{\alpha}) \int_{\sigma_o}^1 \frac{c}{c_{av}} (\sigma - \sigma_o + \sigma_o \cos\gamma) d\sigma \tag{138}$$

Then for the $A \to \infty$ rectangular wing with winglet chord equal to wing chord

$$C_{L_\alpha} = 2\pi \left[\cos\phi_o + (1 - \cos\phi_o)(\cos\gamma + \frac{\psi}{\alpha})\cos\gamma\right] \tag{139}$$

$$\frac{C_{mb_r}}{\alpha} = \frac{\pi}{4} \left[\cos^2\phi_o + (1 - \cos\phi_o)(1 - \cos\phi_o + 2\cos\phi_o \cos\gamma)(\cos\gamma + \frac{\psi}{\alpha})\right] \tag{140}$$

The ratio of equation (140) to (139) gives the bending moment to lift ratio as

$$\frac{C_{mb_r}}{C_L} = \frac{\cos\phi_o \left\{1 + \left[\left(\frac{1-\cos\phi_o}{\cos\phi_o}\right)^2 + 2\left(\frac{1-\cos\phi_o}{\cos\phi_o}\right)\cos\gamma\right]\right\}\left(\cos\gamma + \frac{\psi}{\alpha}\right)}{8\left[1 + \frac{1-\cos\phi_o}{\cos\phi_o}\left(\cos\gamma + \frac{\psi}{\alpha}\right)\cos\gamma\right]} \tag{141}$$

The drag ratio given in equation (124) is the product of the aspect ratio and the drag efficiency factor ratio. As $A \to \infty$, the solution of equation (133) gives

$$\frac{A_p}{A} = \left(8\,\frac{C_{mb_r}}{C_L}\right)^2 \tag{142}$$

where C_{mb_r}/C_L is given in equation (141). For a planar rectangular wing

$$e_p = \frac{1}{\sum_{\substack{n=1 \\ \text{odd}}}^{\infty} \frac{1}{n}} \tag{143}$$

For the nonplanar wing the drag efficiency factor is

$$e = \frac{C_{L_\alpha}{}^2}{\pi A \frac{C_{D_i}}{\alpha^2}}$$

where C_{D_i}/α^2 is obtained from equation (114). The $A \to \infty$ a_n coefficients are presented in equation (96). Combining these equations results in

$$\frac{e_p}{e} = \left(\frac{1 + \frac{1-\cos\phi_o}{\cos\phi_o}\psi_\gamma}{1 + \frac{1-\cos\phi_o}{\cos\phi_o}\psi_\gamma\cos\gamma}\right)^2 \frac{\sum_{\substack{n=1 \\ \text{odd}}}^{\infty} n\left(\frac{a_n}{a_1}\right)^2 + \sum_{\substack{n=1 \\ \text{odd}}}^{\infty} \frac{a_n}{a_1} \sum_{\substack{n^*=1 \\ \text{odd}}}^{\infty} \frac{a_{n^*}}{a_1}\, n^* \frac{4}{\pi} D_{nn^*}}{\sum_{\substack{n=1 \\ \text{odd}}}^{\infty} \frac{1}{n}} \tag{144}$$

where ψ_γ is shortened notation for

$$\psi_\gamma = \cos \gamma + \frac{\psi}{\alpha} \tag{145}$$

The summation in the denominator of equation (144) is a logarithmic infinity. The D_{nn*} summation in ratio to this is negligibly small. Using the a_n coefficients of equation (96), the first summation in the numerator becomes

$$\frac{\sum_{\substack{n=1\\ \text{odd}}}^{\infty} n \left(\frac{a_n}{a_1}\right)^2}{\sum_{\substack{n=1\\ \text{odd}}}^{\infty} \frac{1}{n}} = \frac{\sum_{\substack{n=1\\ \text{odd}}}^{\infty} \frac{1}{n} [\psi_\gamma + (1 - \psi_\gamma)\cos n \phi_o]^2}{[\psi_\gamma + (1 - \psi_\gamma)\cos \phi_o]^2 \sum_{\substack{n=1\\ \text{odd}}}^{\infty} \frac{1}{n}}$$

$$= \frac{1}{[\psi_\gamma + (1 - \psi_\gamma)\cos \phi_o]^2} \left[\psi_\gamma^2 + 2\psi_\gamma (1-\psi_\gamma) \frac{\sum_{\substack{n=1\\ \text{odd}}}^{\infty} \frac{\cos n \phi_o}{n}}{\sum_{\substack{n=1\\ \text{odd}}}^{\infty} \frac{1}{n}} \right.$$

$$\left. + \frac{1}{2} (1 - \psi_\gamma)^2 + \frac{1}{2} (1 - \psi_\gamma)^2 \frac{\sum_{\substack{n=1\\ \text{odd}}}^{\infty} \frac{\cos 2n \phi_o}{n}}{\sum_{\substack{n=1\\ \text{odd}}}^{\infty} \frac{1}{n}} \right]$$

Now

$$\sum_{\substack{n=1\\ \text{odd}}}^{\infty} \frac{\cos n \phi_o}{n} = \frac{1}{2} \ln \left|\cot \frac{\theta_o}{2}\right| \quad , \text{ and } \sum_{\substack{n=1\\ \text{odd}}}^{\infty} \frac{\cos 2n \phi_o}{n} = \frac{1}{2} \ln \left|\cot \phi_o\right|$$

which are finite values for $\phi_o > 0$. Since these terms are divided by infinity the expressions with the cosine summations are hence zero. Equation (144) now simplifies to

$$\frac{e_p}{e} = \frac{1 - 2\psi_\gamma + 3\psi_\gamma^2}{2\cos^2\phi_o\left(1 + \frac{1-\cos\phi_o}{\cos\phi_o}\psi_\gamma\cos\gamma\right)^2} \tag{146}$$

With equation (141) inserted into equation (142), the planar rectangular wing aspect-ratio ratio as $A \to \infty$ becomes

$$\frac{A_p}{A} = \left(8\frac{C_{mb_r}}{C_L}\right)^2 = \cos^2\phi_o\left\{\frac{1 + \left[\left(\frac{1-\cos\phi_o}{\cos\phi_o}\right)^2 + 2\frac{1-\cos\phi_o}{\cos\phi_o}\cos\gamma\right]\psi_\gamma}{1 + \frac{1-\cos\phi_o}{\cos\phi_o}\psi_\gamma\cos\gamma}\right\}^2 \tag{147}$$

Combining equations (124), (146), and (147), the induced drag ratio parameter is

$$\frac{D_i}{D_{ip}} = \frac{1}{2}(1 - 2\psi_\gamma + 3\psi_\gamma^2)\frac{\left\{1 + \left[\left(\frac{1-\cos\phi_o}{\cos\phi_o}\right)^2 + 2\frac{1-\cos\phi_o}{\cos\phi_o}\cos\gamma\right]\psi_\gamma\right\}^2}{\left(1 + \frac{1-\cos\phi_o}{\cos\phi_o}\psi_\gamma\cos\gamma\right)^4} \tag{148}$$

where $\psi_\gamma = \cos\gamma + \psi/\alpha$. Equation (148) is the ratio of the induced drag of a rectangular planar-wing winglet as $A \to \infty$ to the induced drag of a planar rectangular wing of equal root bending moment.

In equation (148), there is a value of ψ/α at which D_i/D_{ip} is minimum. Take the derivative of D_i/D_{ip} with respect to ψ_γ, set to zero, and solve for ψ_γ, to obtain

$$\left.\begin{aligned} \psi_{\gamma_{\substack{min\\D_i}}} &= \frac{2(1 - T^2)}{P + \left[P^2 + 4(1 - T^2)(3 + 3T^2 + 6T\cos\gamma - P)\right]^{1/2}} \\ \left(\frac{\psi}{\alpha}\right)_{\substack{min\\D_i}} &= \psi_{\gamma_{\substack{min\\D_i}}} - \cos\gamma \end{aligned}\right\} \tag{149}$$

where

$$T = \frac{1 - \cos \phi_0}{\cos \phi_0}$$

$$P = 3 - 3T^2 - (3T + T^3) \cos \gamma - 2T^2 \cos^2\gamma \qquad (150)$$

The example configuration has $\phi_0 = 28.125$ degrees. Then

$$T = .13389$$

$$P = 2.94622 - .40406 \cos \gamma - .03585 \cos^2\gamma \qquad (151)$$

$$\psi_{\gamma_{\substack{min \\ D_i}}} = \frac{\psi}{\alpha})_{\substack{min \\ D_i}} \cos \gamma = \frac{1.96415}{P + (P^2 - 3.92830P + 11.99614 + 3.15571 \cos \gamma)^{1/2}} \qquad (152)$$

and equations (148) and (147) become

$$\frac{D_i}{D_{ip}} = \frac{1}{2} (1 - 2\psi_\gamma + 3\psi_\gamma{}^2) \frac{[1 + (.01793 + .26778 \cos \gamma)\psi_\gamma]^2}{(1 + .13389 \psi_\gamma \cos \gamma)^4} \qquad (153)$$

$$\frac{A_p}{A} = (8\frac{C_{mb_r}}{C_L})^2 = .77779 \left[\frac{1 + (.01793 + .26778 \cos \gamma)\psi_\gamma}{1 + .13389 \psi_\gamma \cos \gamma}\right]^2 \qquad (154)$$

Using equations (151) through (154), numerical values can be determined. These values are presented in table VII.

An important wing-winglet condition is to have minimum drag ratio occur when ψ/α is zero. This means that the drag will remain at the bottom of the drag bucket at all values of α; that is, independent of lift. Minimum drag results when the conditions of equation (149) are fulfilled. When $\psi/\alpha = 0$, $\psi_{\gamma_{min\ Di}}$ equals $\cos \gamma$, then solving equation (149) for $\cos \gamma$ leads to a fourth degree polynomial in $\cos \gamma$, given by

$$2T^2\cos^4\gamma + (9T-2T^2 +T^3) \cos^3\gamma - (3T-6T^2 +T^3) \cos^2\gamma + 3(1-T^2)\cos \gamma - 1+T^2= 0 \qquad (155)$$

For the example configuration ϕ_o = 28.125 degrees, then T = .13389, and the solution of equation (155) for cos γ results in

$$\left.\begin{aligned} \cos\gamma &= .32987 \\ \gamma &= 70.74 \text{ degrees} \\ \frac{D_i}{D_{ip}} &= .33705 \\ \frac{A_p}{A} &= \left(8\frac{C_{mb_r}}{C_L}\right)^2 = .80951 \\ \frac{\psi}{\alpha} &= 0 \end{aligned}\right\} \qquad (156)$$

in which D_i/D_{ip} and A_p/A are evaluated with ψ_γ = cos γ in equations (153) and (154).

Slender wing with $\gamma = 0$. - Since D_{nn*} coefficients are zero when $\gamma = 0$, then from equations (90), (92), and (93) for the slender wing

$$\frac{a_n}{a_1} = \frac{1}{n}\,\frac{\frac{2}{\pi}\left[\frac{\sin(n-1)\,\phi_o}{n-1} - \frac{\sin(n+1)\,\phi_o}{n+1}\right]\frac{\psi}{\alpha}}{1 + \frac{2}{\pi}\left(\phi_o - \sin\phi_o\cos\phi_o\right)\frac{\psi}{\alpha}} \qquad (157)$$

$$\frac{a_1}{\alpha} = 1 + \frac{2}{\pi}\left(\phi_o - \sin\phi_o\cos\phi_o\right)\frac{\psi}{\alpha} \qquad (158)$$

For γ = 0, equations (55), (59), and (66) with equation (157) can be written as

$$\frac{C_{mb_r}}{C_L} = \frac{1}{3\pi}\left(1 + \frac{3k_1\frac{\psi}{\alpha}}{1 + k_o\frac{\psi}{\alpha}}\right) \qquad (159)$$

$$e = 1 + k_2\left(\frac{\frac{\psi}{\alpha}}{1 + k_o\frac{\psi}{\alpha}}\right)^2 \qquad (160)$$

where

$$k_0 = \frac{2}{\pi}(\phi_0 - \sin\phi_0 \cos\phi_0)$$

$$k_1 = \frac{2}{\pi}\sum_{\substack{n=3\\ \text{odd}}}^{\infty} \frac{(-1)^{\frac{n+1}{2}}}{(n^2-4)\,n}\left[\frac{\sin(n-1)\,\phi_0}{n-1} - \frac{\sin(n+1)\,\phi_0}{n+1}\right] \tag{161}$$

$$k_2 = \left(\frac{2}{\pi}\right)^2 \sum_{\substack{n=3\\ \text{odd}}}^{\infty} \frac{1}{n}\left[\frac{\sin(n-1)\,\phi_0}{n-1} - \frac{\sin(n+1)\,\phi_0}{n+1}\right]^2$$

As aspect ratio approaches zero, η_{cp} becomes $4/3\pi$, and $e_p = 1$, then equations (123) and (124) for $A \to 0$, $\gamma = 0$, but for arbitrary values of ϕ_0 and ψ/α, become

$$\frac{A_p}{A} = \left(3\pi \frac{C_{mb_r}}{C_L}\right)^2 = \left(1 + \frac{3k_1 \frac{\psi}{\alpha}}{1 + k_0 \frac{\psi}{\alpha}}\right)^2 \tag{162}$$

$$\frac{D_i}{D_{ip}} = \left(1 + \frac{3k_1 \frac{\psi}{\alpha}}{1 + k_0 \frac{\psi}{\alpha}}\right)^2 \left[1 + k_2 \left(\frac{\frac{\psi}{\alpha}}{1 + k_0 \frac{\psi}{\alpha}}\right)^2\right] \tag{163}$$

This function in equation (163) results in a drag bucket along ψ/α. Take the derivative of D_i/D_{ip} with respect to ψ/α, set to zero, and solve for ψ/α, gives

$$\left(\frac{\psi}{\alpha}\right)_{\substack{\min\\ D_i}} = \frac{-1}{\frac{1}{6}\frac{k_2}{k_1}\left[1 + \left(1 - 72\left(\frac{k_1}{k_2}\right)^2\right)^{1/2}\right] + k_0} \tag{164}$$

Inserting equation (164) into (163) gives the equation for minimum drag as

$$\frac{D_i}{D_{ip}} = \frac{5}{8}\left[1 + \frac{k_2}{180\ k_1^2} - \frac{18}{5}\ \frac{k_1^2}{k_2} + \left(\frac{2}{5} - \frac{k_2}{180\ k_1^2}\right)\left(1 - 72\ \frac{k_1^2}{k_2}\right)^{1/2}\right] \qquad (165)$$

where k_1 and k_2 are functions of only ϕ_o, as can be seen in equation (161).

With ϕ_o = 28.125 degrees, the k_o, k_1, k_2 from equation (161) are

$$k_o = .047835, \qquad k_1 = .006857, \qquad k_2 = .009080$$

then from equations (164), (165), and (162)

$$\left(\frac{\psi}{\alpha}\right)_{\substack{min \\ D_i}} = -2.25573$$

$$\frac{D_i}{D_{ip}} = .95084 \qquad (166)$$

$$\frac{A_p}{A} = .89868, \quad \frac{C_{mb_r}}{C_L} = .10058$$

For the condition γ = 0, ϕ_o = 28.125 degrees, values from equations (157), (158), (159), (160), (162), and (163) are presented in tables V and VI.

RESULTS AND DISCUSSION

Load-Line and Slender Wing Theory

Analytically, these are two-dimensional theories. That is, only induced velocities normal to the surface in the yz-plane enter into the solution. Longitudinal effects enter the problem only insofar as wing chord distribution in the load-line method influences the solution. The load-line solution is for wings with the one-half chord line straight or unswept in the yz-plane. However, swept wing parameters, developed in a following section, approximate swept planform geometry effects for solution with load-line theory. Because of the quasi two-demensional nature of these theories, they are ideally suited for the more complex type of loading solutions (such as, taking into account nonplanar effects, interference effects of multiplanes, fuselage-by-image methods, wing-in-jet, ground, tunnel walls, or passing through trailing vortices of another aircraft). This is because the load-line method is quasi two-dimensional, hence, in many cases, the additional normal-to-surface induced velocity due to the added configuration likewise may be determined for two-dimensional flow. Because the boundary conditions are satisfied at all points with the load-line and slender wing theories, the spanwise loading can be predicted accurately for any complex spanwise distribution of wing surface inclination (such as winglet toe-in angles, control surface deflections, twist, induced angles due to other wings, fuselage, wing-in-jet, ground, or free vortex). The introduction of the induced-angle parameter k of equation (24) transforms lifting line theory effectively into a lifting surface theory, or load-line theory, for the prediction of spanwise loading characteristics. The integrated lift is accurate since the definition of k depended on this lift.

Swept wing approximation for load-line theory. - Load-line theory can be made applicable to swept wings by a redefinition of the aspect ratio and wing chord distribution parameters. From simple sweep theory concept of flow normal to wing, the effective aerodynamic semispan of the swept wing is given by the distance along the midchord line from wing root to wing tip denoted by s_{e_Λ}. Then the effective aspect ratio and lift parameters are

$$A_\Lambda = \frac{2s_{e\Lambda}}{c_{av}} = \frac{s_{e\Lambda}}{s_e}\frac{2s_e}{c_{av}} = \frac{s_{e\Lambda}}{s_e} A; \text{ and } C_{L_\Lambda} = \frac{s_{e\Lambda}}{s_e} C_L \tag{167}$$

Equation (167) applies to a sweep angle that varies along the span, such as that for a cranked wing. For a constant sweep angle, $s_{e\Lambda}/s_e = \cos \Lambda$, then

$$A_\Lambda = A/\cos \Lambda; \qquad C_{L_\Lambda} = C_L/\cos \Lambda \tag{168}$$

where Λ is the sweep angle of the wing one-half chord line.

In addition to the swept-wing parameters of equations (167) and (168), the swept wing needs a spanwise wing chord factor which relates wing sweep angle to wing taper ratio. Shown in figure 21 of reference 9 is a curve of taper ratio as a function of sweep angle. Wings with this sweep and taper ratio have approximately elliptical spanwise loading independent of aspect ratio. This curve was analyzed for the present study with the results

$$\lambda = .375 \frac{1 - \sin \Lambda}{1 + \sin \Lambda} \tag{169}$$

Equation (169) forms the basis for defining the equivalent chord distribution of a straight wing which will give a spanwise loading distribution similar to that of the swept wing. The effective chord distribution is of the form

$$\left(\frac{c}{c_{av}}\right)_e = \frac{1 - \sin \Lambda + 2|\sigma| \sin \Lambda}{1 - \sin \Lambda + 2\sigma_{cc} \sin \Lambda} \frac{c}{c_{av}} \tag{170}$$

where the center of spanwise chord distribution is

$$\sigma_{cc} = \int_0^1 \sigma \frac{c}{c_{av}} d\sigma \tag{171}$$

$$\underset{\text{ellipse}}{=} \frac{4}{3\pi} \qquad \underset{\text{straight taper}}{=} \frac{1 + 2\lambda}{3 + 3\lambda}$$

When $\sigma = 1$, $c = c_t$, and, when $\sigma = 0$, $c = c_r$. These values are inserted into equation (170), and a ratio made; then equation (170) becomes equation (169) when $\lambda_e = .375$. Equations (167), (168), and (170) provide swept wing load-line theory replacement parameters which are read as

$$\left.\begin{array}{l}\text{for A in load-line theory, substitute } s_{e\Lambda}\, A/s_e \text{ or } A/\cos\Lambda \\ \text{for } C_L \text{ in load-line theory, substitute } s_{e\Lambda} C_L/s_e \text{ or } C_L/\cos\Lambda \\ \text{for } c/c_{av} \text{ in load-line theory, substitute } (c/c_{av})_e \text{ of equation (170)}\end{array}\right\} \quad (172)$$

The chord conditions given in equation (170) provide an interesting relationship for swept wings which have elliptical additional spanwise loading distribution. For the unswept elliptic planform, $(c/c_{av})_e = (4/\pi)(1-\sigma^2)^{1/2}$. Then the chord distribution for swept wings is

$$\frac{c}{c_{av}} = \frac{\frac{4}{\pi}(1-\sigma^2)^{1/2}\left[1-\left(1-\frac{8}{3\pi}\right)\sin\Lambda\right]}{1-\sin\Lambda+2\sigma\sin\Lambda} \quad (173)$$

For the chord distribution given in equation (173), the swept-wing aerodyanmic characteristics are given by the elliptic wing results of equation (46), provided A is replaced by $A/\cos\Lambda$ and C_L by $C_L/\cos\Lambda$.

Rectangular Wing Winglet, $\phi_o = 5\pi/32$, $\lambda_{wo} = 1$

Example solutions for the aerodynamic characteristics of this configuration are shown in the previous chapter. Results, including influence coefficients and force and moment coefficients, are presented in tables I through VII. Examination of table VI shows that, compared to a planar elliptic wing of equal lift and equal wing root bending moment, the drag ratio for the wing-winglet is about 5% less when $A \to 0$, about 10% greater for $A = 10.94$, and infinitly greater as $A \to \infty$. Comparing with a planar wing with same rectangular planform shows definite drag buckets at all aspect ratios. The induced drag ratio, ratio of aspect ratio, and wing root bending moment data of tables VI and VII are presented in figure 2 as functions of winglet toe-in angle. The induced drag ratio curves of figure 2(a) have drag buckets with

respect to toe-in angle. These buckets are shallow and wide for the low aspect ratio wing but become deep and narrow as aspect ratio becomes large. At minimum induced drag ratio, the comparative reduction of induced drag is about 4% at $A \to 0$, 11% at $A = 10.94$, and 66% at $A \to \infty$. The position of the drag bucket along the ψ/α axis in figure 2(a) is strongly influenced by the winglet dihedral cant angle γ. It is also influenced by the ratio of winglet chord to wing chord. This characteristic is useful for configuration design since, when a value of ψ/α and winglet chord are specified, γ is defined by the minimum induced drag condition.

Curves of ratios of wing root bending moment coefficient to lift coefficient are presented in figure 2(b). These values apply to both the wing-winglet and planar-wing configurations since the condition for comparison was that lift and root bending moment be the same. The C_{mb_r}/C_L ratio becomes smaller as aspect ratio and toe-in angle decrease and as dihedral cant angle increases. The aspect ratio of the planar rectangular wing in terms of that of the rectangular wing-winglet is given in figure 2(c). This is the aspect ratio the planar wing must have in order to give the same lift and wing bending moment as the wing-winglet with higher aspect ratio. It can be recalled that the wing-winglet aspect ratio definition is based on total spanwise distance along wing and winglet and total surface area which includes wing area plus winglet area. The values of figure 2(c) correspond through A, ψ/α, and γ with those of figures 2(a) and (b). Figure 3 results from cross plotting the values of figure 2. The decrease in wing root bending moment coefficient as the winglet approaches the up position is shown clearly in figure 3. For $A = 10.94$ at $\gamma = 90$ degrees the root bending moment is 4.3% less, however, induced drag ratio is 3.4% more than that at $\gamma = 0$ degrees. The planar rectangular wing induced drag D_{i_p} is not a constant in the D_i/D_{i_p} ratio but varies with the planar wing aspect ratio A_p. The value of A_p was specified under the conditions that lift and wing root bending moment of the planar wing equal that of the nonplanar wing. Curves of only the rectangular wing winglet induced drag versus wing root bending moment are presented in figure 4. The induced-drag parameter is $e^{-1} = \pi A\, C_{D_i}/C_L{}^2$, aspect ratio is 10.94, and the lift of the various configurations is the same. As shown in figure 4, at low values of

root bending moment, the induced drag is marginally less at high values of dihedral cant angle. The flat winglet $\gamma = 0$ configuration curve almost envelopes the higher γ angled curves. However, the $\gamma = 0$ curve is characterized by large negative values of ψ/α which become less negative as angle of attack increases resulting in larger root bending moment coefficients.

A deep and narrow drag bucket means that induced drag is sensitive to changes in ψ/α. Thus, when a design toe-in angle is specified, any change in angle of attack or lift will alter the ψ/α ratio and induced drag rises up the side of the drag bucket. In this regard, the ideal would be zero toe-in angle; then the ψ/α ratio remains the same at any lift. The dihedral cant angle γ has a valuable asset in that it influences the position of the induced drag bucket along the ψ/α axis. Then γ can be chosen such that minimum induced drag ratio can be obtained with minimum ψ/α ratio. Examination of figure 2(a) indicates that, for this wing winglet configuration, the minimum induced drag for $\psi/\alpha = 0$ occurs at $\gamma = 71$ degrees as $A \to \infty$, and at $\gamma = 90$ degrees for $A = 10.94$. In view of this characteristic a good $A = 10.94$ rectangular wing winglet has $\gamma = 90$ degrees, $\psi/\alpha = 0$, and minimum induced drag. For example, a designer has proposed an aspect ratio equal to nine planar rectangular wing, and asks if drag can be reduced without altering wing root bending moment. From figure 2(c), when $A_p = 9$, $\psi/\alpha = 0$, $\gamma = 90$, then $A = 10.94$. The bending moment coefficient from figure 2(b) is $C_{mb_r}/C_L = .1041$ which leads to the same root bending moment as that of the planar rectangular wing. The induced drag ratio from figure 2(a) is $D_i/D_{ip} = .899$. Thus, the designer has an alternative configuration which has 10.1% less induced drag, the same wing root bending moment, and equal surface area. Since surface areas are the same, friction drag is approximately the same for planar wing and wing winglet configurations. This wing winglet configuration is with winglet starting at $\phi_o = 5\pi/32$ span station. The effect of other winglet sizes needs to be investigated for establishing an optimum.

The swept wing approximation equations can be applied to the rectangular wing winglet example. In the rectangular wing solution, $(c/c_{av})_e$ of equation (170) was unity. Then

$$\frac{c}{c_{av}} = \frac{1 - \sin \Lambda + 2\, \sigma_{cc} \sin \Lambda}{1 - \sin \Lambda + 2\, |\sigma| \sin \Lambda} \tag{174}$$

where σ_{cc} is given in equation (171). Inserting equation (174) into equation (171) and solving for σ_{cc} gives

$$\sigma_{cc} = \frac{1}{2 \tanh^{-1} \sin \Lambda} - \frac{1 - \sin \Lambda}{2 \sin \Lambda} \tag{175}$$

then equation (174) becomes

$$\frac{c}{c_{av}} = \frac{(\tanh^{-1} \sin \Lambda)^{-1} \sin \Lambda}{1 - \sin \Lambda + 2\, |\sigma| \sin \Lambda} \tag{176}$$

where Λ is the half chord line sweep angle. As an example with $\Lambda = 30$ degrees

$$\frac{c}{c_{av}} = \frac{1.8205}{1 + 2\, |\sigma|} \tag{177}$$

which is not a straight-tapered wing. However, a mean taper ratio is approximately $\lambda = 0.29$. From equation (172) with $\Lambda = 30$ degrees and $A = 10.94$ the swept wing aspect ratio is $A = 9.47$, and swept wing lift coefficient is 0.866 times that of the rectangular wing winglet. Thus, in this example, the $A = 10.94$ rectangular wing winglet results of figures 2, 3, and 4 apply equally to a 30 degree sweptback wing winglet of aspect ratio 9.47, with approximately a taper ratio of 0.29.

CONCLUDING REMARKS

A goal for the nonplanar wing loading theories developed in the present report was to satisfy boundary conditions of the wing analytically at all points. This goal was attained by Fourier analyses which permits integration of wing chord and wing inclination boundary conditions which specify no flow through the wing. The nonplanar load line, slender wing,

elliptic wing, and infinite aspect ratio limit theories have proved to be useful tools for applications in loading aerodynamics. They give lifting surface accuracy with lifting line theory simplicity, that is, they remain quasi two-dimensional solution methods. Because the boundary conditions are satisfied at all points, the spanwise loading circulation can be predicted accurately for complex spanwise distribution of angle of attack such as that due to winglet or control surface deflections, wing twist, induced angles by multiwings, multiwinglets, ground, walls, jet, or fuselage. Because of the quasi two-dimensional nature of these theories they are well suited for these complex type of loading solutions, since, in many cases, the induced angles normal to the surface due to the added configurations are likewise determined for two-dimensional flow. Force and moment coefficients of nonplanar wings involve integrations along the nonplanar surface of loading circulation vectors relative to the surface. Equations for nonplanar wing lift, running wing bending moment, rolling, and induced drag coefficients are developed. The nonplanar wing induced drag coefficient is equal to the planar wing induced drag expression plus a summation of products of wing circulation Fourier coefficients and nonplanar induced drag influence coefficients. These influence coefficients are functions of the nonplanar curve of the wing but are independent of any other wing geometry parameter. Swept wing parameters are approximated for wing chord and aspect ratio. These are used in the load line method for obtaining nonplanar swept wing solutions.

Example application of these theories have been made for a rectangular wing with wingtip winglets. In this example configuration the winglet extends from span station .882 to 1, and winglet chord equals wing chord. The thirty-degree swept wing planform equivalent to the rectangular wing has a taper ratio of about 0.29. Compared with a planar rectangular wing of equal lift and root bending moment, the winglet wing has minimum induced drag ratios of .948, .869, and .336 at aspect ratios of 0, 10.94, and ∞, respectively. The study of this example shows that there is just a deep a drag bucket with

winglet planar, but with negative deflection, as with the winglet up at high dihedral cant angle. However, it was found that dihedral cant angle has a valuable asset in that for the optimized design configuration the drag at the bottom of the drag bucket can be realized for any wing angle of attack or lift, whereas for the planar winglet the drag rises up the side of the drag bucket as angle of attack increases or decreases.

Vought Corporation Hampton Technical Center
Hampton, Virginia 23666
March 21, 1977

REFERENCES

1. von Karman, Theodore; and Burgers, J. M.: General Aerodynamic Theory - Perfect Fluids, Vol. II of Aerodynamic Theory, div. E, W. F. Durand, ed., First Dover edition, Dover Publications, New York, 1963. pp. 201-236.

2. Cone, Clarence D. Jr.: The Theory of Induced Lift and Minimum Induced Drag of Nonplanar Lifting Systems. NASA TR R-139, 1962.

3. Whitcomb, Richard T.: A Design Approach and Selected Wind-Tunnel Results of High Subsonic Speeds for Wing-Tip Mounted Winglets. NASA TN D-8260, 1976.

4. Ashley, Holt; and Landahl, Martin: Aerodynamics of Wing and Bodies. Addison-Wesley Publishing Company, Inc., Reading, Mass., 1965. pp. 208-226.

5. Heyson, Harry H.; Riebe, Gregory D.; and Fulton, Cynthia L.: Theoretical Parametric Study of the Relative Advantages of Winglets and Wing-Tip Extensions. NASA TM X-74003, 1977.

6. DeYoung, John: Wing Loading Theory Satisfying All Boundary Points, Ph.D. Dissertation, The University of Texas at Arlington, Arlington, Texas, Dec. 1975.

7. DeYoung, John: Rule of Thumb Equation for Predicting Lifting-Surface Theory Values of Lift. Jour. of the Aeronautical Sciences, Vol. 24, No. 8, Aug. 1957. p. 629.

8. DeYoung, John: Spanwise Loading for Wings and Control Surfaces of Low Aspect Ratio. NACA TN 2011, Jan. 1950.

9. DeYoung, John; and Harper, Charles W.: Theoretical Symmetric Span Loading at Subsonic Speeds for Wings Having Arbitrary Plan Form. NACA Report 921, 1948.

TABLE I. - $L_{n^*_w}$ COEFFICIENTS FOR EQUATIONS (41) AND (71) OF PLANAR-WING WINGLET WITH $\phi_0 = 5\pi/32$ AND M=15

γ deg	n* \ w	1	2	3	4	5	6	7	8
90	1	.01931	.13347	-.11359	.04958	.03096	.01885	.01361	.01221
	3	-.04873	-.16124	-.10834	.03594	.02439	.01516	.01104	.00993
	5	.04879	-.05402	-.09461	.01476	.01390	.00921	.00687	.00624
	7	.02698	.07104	-.06937	-.00490	.00349	.00319	.00261	.00246
	9	-.02714	.06417	-.03415	-.01567	-.00341	-.00101	-.00042	-.00025
	11	-.02089	-.01173	.00316	-.01888	-.00542	-.00256	-.00163	-.00135
75	1	.00066	.08511	-.06993	.03114	.02046	.01291	.00951	.00858
	3	-.02812	-.11212	-.06670	.02232	.01600	.01033	.00769	.00696
	5	.03297	-.02911	-.05830	.01264	.00891	.00627	.00473	.00433
	7	.01538	.04714	-.04294	-.00384	.00192	.00202	.00173	.00165
	9	-.01795	.03687	-.02156	-.01048	-.00262	-.00086	-.00039	-.00025
	11	-.01296	-.01042	.00110	-.00982	-.00381	-.00186	-.00120	-.00100

TABLE II. - $n^*\frac{4}{\pi} D_{nn^*}$ COEFFICIENTS FOR EQUATIONS (69) AND (93) OF PLANAR-WING WINGLET WITH $\phi_0 = 5\pi/32$

γ deg	n \ n*	1	3	5	7	9	11
90	1	.03335	.00666	-.00167	-.01243	-.06192	-.10534
	3	-.00333	-.17809	-.16927	-.05646	-.02895	-.06658
	5	-.00258	-.16334	-.09138	.08085	.11343	.03307
	7	.03630	.02441	.11900	.18434	.11512	-.00789
	9	.03156	.12523	.17174	.08391	-.03334	-.07625
	11	-.02442	.06277	.04171	-.11282	-.16333	-.02769
75	1	.02254	.01464	.00887	-.00752	-.04600	-.06860
	3	-.02833	-.11801	-.09743	-.03368	-.02510	-.04331
	5	-.02362	-.10743	-.05579	.05572	.06810	.01018
	7	.02184	.01044	.07264	.11569	.06939	-.01221
	9	.01822	.08039	.10960	.04817	-.02089	-.03748
	11	-.01661	.04548	.02751	-.07520	-.09798	-.00506

TABLE III. - $n^* \frac{4}{\pi} K_{nn^*}$ COEFFICIENTS FOR EQUATIONS (39) AND (87) OF RECTANGULAR WING WINGLET WITH $\phi_o = 5\pi/32$ AND $\lambda_{wo} = 1$

γ deg	n \ n*	1	3	5	7	9	11
90	1	.03511	-.06588	-.04584	.00025	-.05336	-.12659
	3	.01535	-.32053	-.22541	.01423	-.00065	-.13283
	5	.02287	-.30001	-.09515	.20900	.15731	-.04113
	7	.06097	-.02873	.21046	.32421	.12296	-.08051
	9	.03951	.15523	.31146	.14626	-.12323	-.14249
	11	-.04557	.11283	.14343	-.17091	-.34193	-.06549
75	1	.02294	-.04218	-.01601	.00123	-.04333	-.08389
	3	.00757	-.20220	-.12487	.01266	-.01483	-.09166
	5	.01103	-.19751	-.05132	.13694	.08803	-.03467
	7	.03396	-.02045	.13428	.20153	.06996	-.05948
	9	.01968	.10354	.19886	.08172	-.07742	-.07450
	11	-.03292	.08485	.09031	-.11774	-.20657	-.02172

TABLE IV. - $n^* \frac{4}{\pi} I_{nn^*}$ COEFFICIENTS FOR EQUATIONS (39) AND (87) OF RECTANGULAR WING

n \ n*	1	3	5	7	9	11
1	1	1	1	1	1	1
3	1/3	4.6	3.3809	3.17778	3.10390	3.06838
5	1/5	2.02857	8.93651	6.14748	5.59620	5.37314
7	1/7	1.36191	4.39105	13.68594	9.19620	8.22020
9	1/9	1.03463	3.10900	7.15260	18.72562	12.46581
11	1/11	.81368	2.44234	5.23103	10.19930	23.98962

TABLE V. - EXAMPLE LOADING CHARACTERISTICS SOLUTIONS OF RETANGULAR WING WINGLET WITH $\phi_o = 5\pi/32$ AND $\lambda_{wo} = 1$

Υ deg	$\frac{\Psi}{\alpha}$	A	a_1/α	a_3/a_1	a_5/a_1	a_7/a_1	a_9/a_1	C_{L_α}	$\frac{C_{mb_r}}{\alpha}$	$\frac{C_{Di}}{\pi A\alpha^2}$	e
90	-1	→ 0	.8761	-.0978	-.0634	-.0168	.0056	1.339A	.1304A	.2081	.8733
		10.94	.2480	-.1378	-.2178	-.1059	.0127	4.263	.4261	.0217	.7094
		→ ∞	3.055/A	-.3508	-.6666	-.5449	-.2299				
	-.25	10.94	.2640	-.0168	-.1124	-.0569	.0087	4.4100	.4546	.0195	.8440
	0	→ 0	.9217	-.0463	-.0317	-.0057	.0011	1.393A	.1379A	.2219	.8857
		10.94	.2690	.0236	-.0772	-.0405	.0074	4.446	.4626	.0195	.8608
		→ ∞	3.528/A	.0370	-.1753	-.1550	-.0366				
	1	→ 0	.9672	.0003	-.0029	.0043	-.0031	1.447A	.1453A	.2418	.8769
		10.94	.2901	.1614	.0431	.0154	.0028	4.615	.4963	.0235	.7690
		→ ∞	4/A	1/3	1/5	1/7	1/9				
75	-1	→ 0	.9038	-.0786	-.0491	-.0210	.0064	1.387A	.1372A	.2151	.9066
		10.94	.2547	-.0889	-.1754	-.0927	.0116	4.348	.4421	.0203	.7877
		→ ∞	3.178/A	-.2395	-.5255	-.4329	-.1743				
	-.5	→ 0	.9261	-.0548	-.0342	-.0155	.0044	1.416A	.1413A	.2224	.9136
		10.94	.2652	-.0135	-.1091	-.0610	.0097	4.460	.4639	.0194	.8674
		→ ∞	3.414/A	-.0467	-.2814	-.2392	-.0783				
	0	→ 0	.9463	-.0311	-.0194	-.0100	.0025	1.441A	.1451A	.2294	.9154
		10.94	.2750	.0620	-.0427	-.0293	.0078	4.581	.4905	.0198	.8964
		→ ∞	3.650/A	.1211	-.0689	-.0705	.0053				
0	-2.256	→ 0	.8911	-.1002	-.0645	-.0281	-.0018	1.400A	.1407A	.2097	.9466
	-2	10.94	.2475	-.1037	-.1905	-.1015	.0100	4.251	.4320	.0197	.7772
	-1.25	10.94	.2651	-.0064	-.1038	-.0582	.0089	4.553	.4863	.0189	.9272
	-1	→ 0	.9522	-.0412	-.0265	-.0116	-.0007	1.496A	.1553A	.2288	.9906
		10.94	.2706	.0260	-.0750	-.0438	.0086	4.648	.5045	.0191	.9577
		→ ∞	3.528/A	.0371	-.1753	-.1550	-.0365				
	0	→ 0	1	0	0	0	0	.5πA	A/6	1/4	1
		10.94	.2914	.1556	.0405	.0139	.0071	5.005	.5779	.0230	.9236
		→ ∞	4/A	1/3	1/5	1/7	1/9				

TABLE VI. - COMPARISON OF INDUCED DRAG OF RECTANGULAR WING WINGLET, $\phi_o = 5\pi/32$, $\lambda_{wo} = 1$, WITH PLANAR WING OF EQUAL LIFT AND EQUAL WING ROOT BENDING MOMENT

γ deg	$\frac{\psi}{\alpha}$	A	e	$\frac{C_{mb_r}}{C_L}$	Planar elliptic wing, $e_p=1$		Compared with planar rectangular wing		
					A_p/A	D_i/D_{ip}	e_p	A_p/A	D_i/D_{ip}
90	-1	→ 0	.8733	.0974	.8421	.9642	1	.8421	.9642
		10.94	.7094	.1000	.8874	1.2509	.9470	.7664	1.0231
	-.25	10.94	.8440	.1031	.9440	1.1185	.9393	.8111	.9028
	0	→ 0	.8857	.0990	.8702	.9825	1	.8702	.9825
		10.94	.8608	.1041	.9618	1.1173	.9380	.8252	.8993
	1	→ 0	.8769	.1005	.8965	1.0224	1	.8965	1.0224
		10.94	.7691	.1075	1.0270	1.3354	.9334	.8768	1.0642
75	-1	→ 0	.9066	.0989	.8687	.9583	1	.8687	.9583
		10.94	.7877	.1017	.9184	1.1658	.9412	.7907	.9448
	-.5	→ 0	.9136	.0998	.8846	.9683	1	.8846	.9683
		10.94	.8674	.1040	.9612	1.1082	.9381	.8248	.8920
	0	→ 0	.9154	.1007	.9007	.9840	1	.9007	.9840
		10.94	.8964	.1071	1.0181	1.1358	.9340	.8698	.9063
0	-2.256	→ 0	.9466	.1005	.8977	.9483	1	.8977	.9483
	-2	10.94	.7772	.1016	.9175	1.1804	.9413	.7900	.9568
	-1.25	10.94	.9272	.1068	1.0136	1.0931	.9343	.8662	.8729
	-1	→ 0	.9906	.1038	.9572	.9664	1	.9572	.9664
		10.94	.9577	.1086	1.0467	1.0929	.9321	.8924	.8685
	0	→ 0	1	.1061	1	1	1	1	1
		10.94	.9236	.1155	1.1842	1.2822	.9236	1	1

TABLE VII. - COMPARISON OF INDUCED DRAG OF $A \to \infty$ RECTANGULAR WING WINGLET, $\phi_o = 5\pi/32$, $\lambda_{wo} = 1$, WITH PLANAR RECTANGULAR WING OF EQUAL LIFT AND EQUAL WING ROOT BENDING MOMENT

	D_i/D_{ip}								
γ, deg \ ψ/α	-1.25	-1.00	-.50	-.25	0	.25	.50	.75	1.00
90			1.3505	.8362	.5000	.3468	.3818	.6098	1.0362
75			.8284	.4915	.3447	.3860	.6198	1.0501	
0	.8337	.5000	.3780	.5971	1.0000				
	A_p/A or $(8\ C_{mb_r}/C_L)^2$								
90			.7639	.7708	.7778	.7848	.7918	.7988	.8059
75			.7580	.7785	.7989	.8192	.8394	.8596	
0	.7179	.7778	.8924	.9471	1.0000				

MINIMUM DRAG AND CONDITIONS FOR MINIMUM DRAG, $A \to \infty$

γ, deg	105	90	75	60	45	30	15	0	70.74
ψ/α	.5582	.3294	.0709	-.1697	-.3761	-.5343	-.6338	-.6677	0
A_p/A	.7691	.7870	.8047	.8210	.8364	.8457	.8524	.8547	.8095
C_{mb_r}/C_L	.1096	.1109	.1121	.1133	.1143	.1150	.1154	.1156	.1125
D_i/D_{ip}	.3373	.3373	.3371	.3368	.3364	.3361	.3359	.3358	.3371

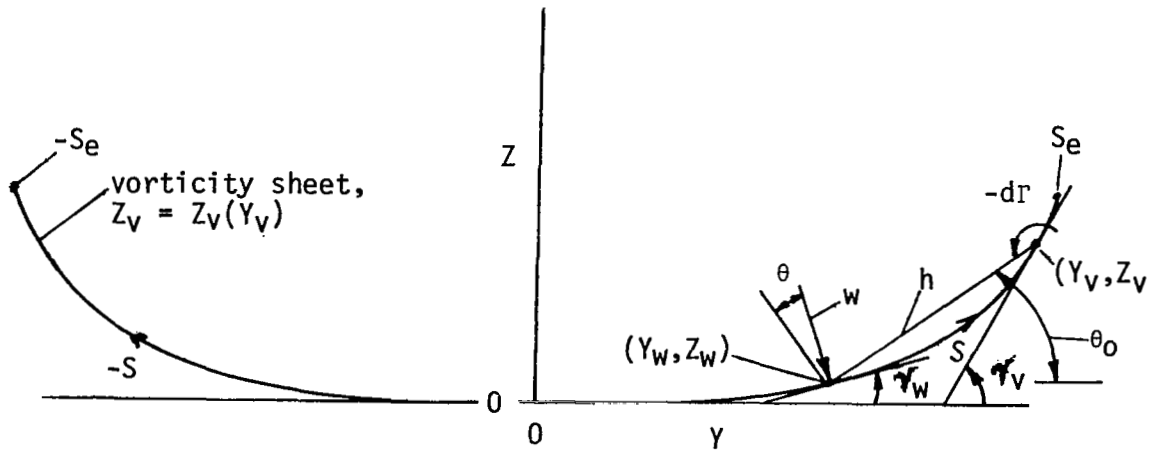

(a) Single nonplanar vorticity sheet.

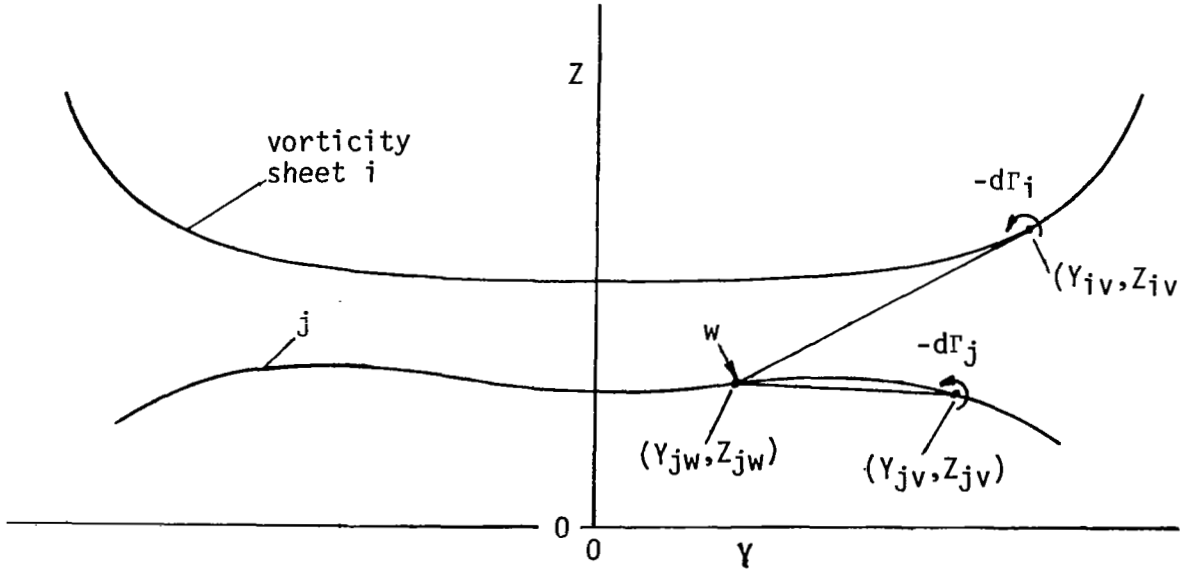

(b) Multiple nonplanar vorticity sheets.

Figure 1. - Coordinate system in yz plane of nonplanar trailing vorticity sheets which extend longitudinally unaltered from zero to infinity.

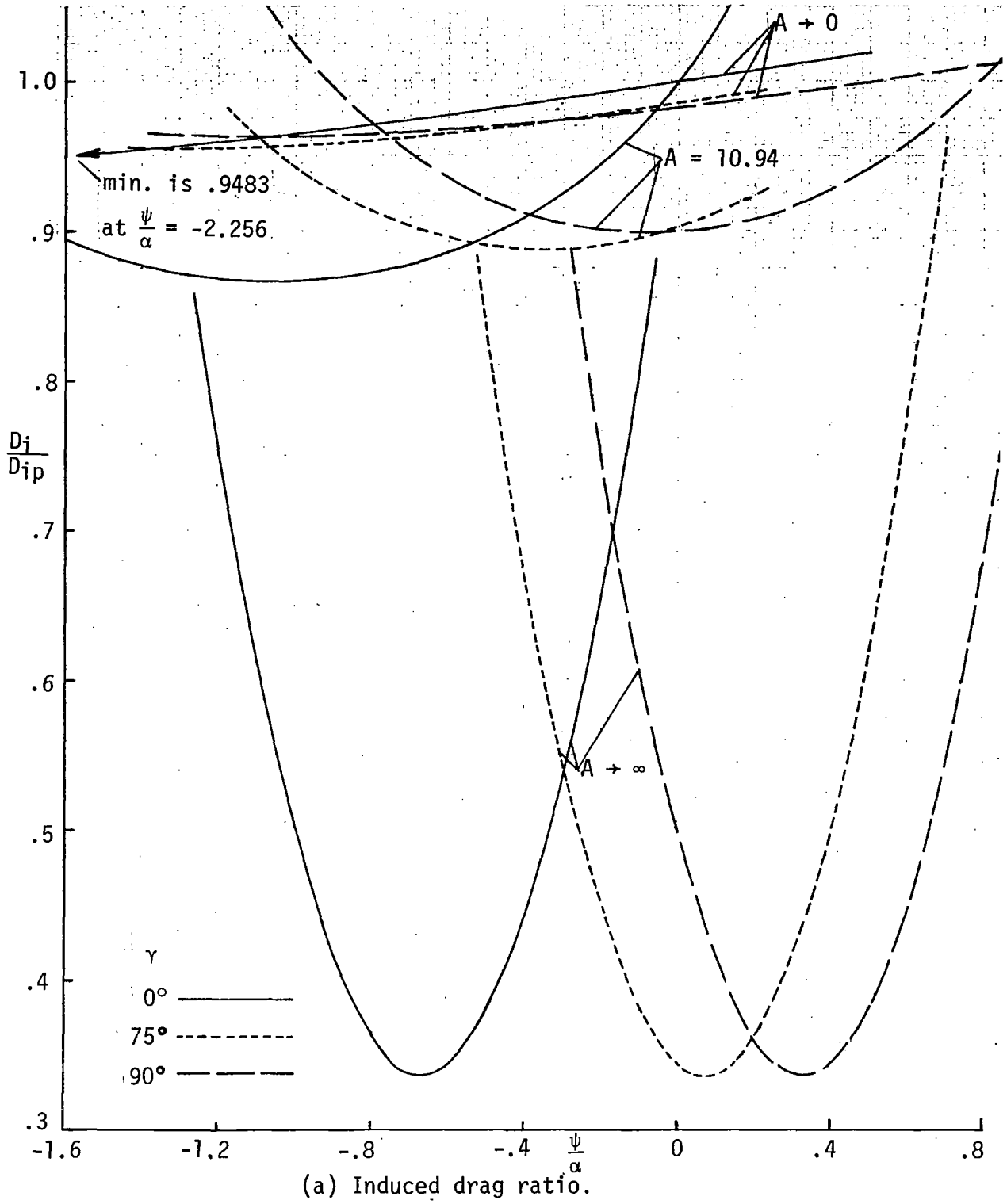

(a) Induced drag ratio.

Figure 2. - Characteristics of rectangular wing winglet, $\phi_o = 5\pi/32$, $\lambda_{wo} = 1$, compared with planar rectangular wing of equal lift and equal wing root bending moment. Subscript p refers to planar wing value

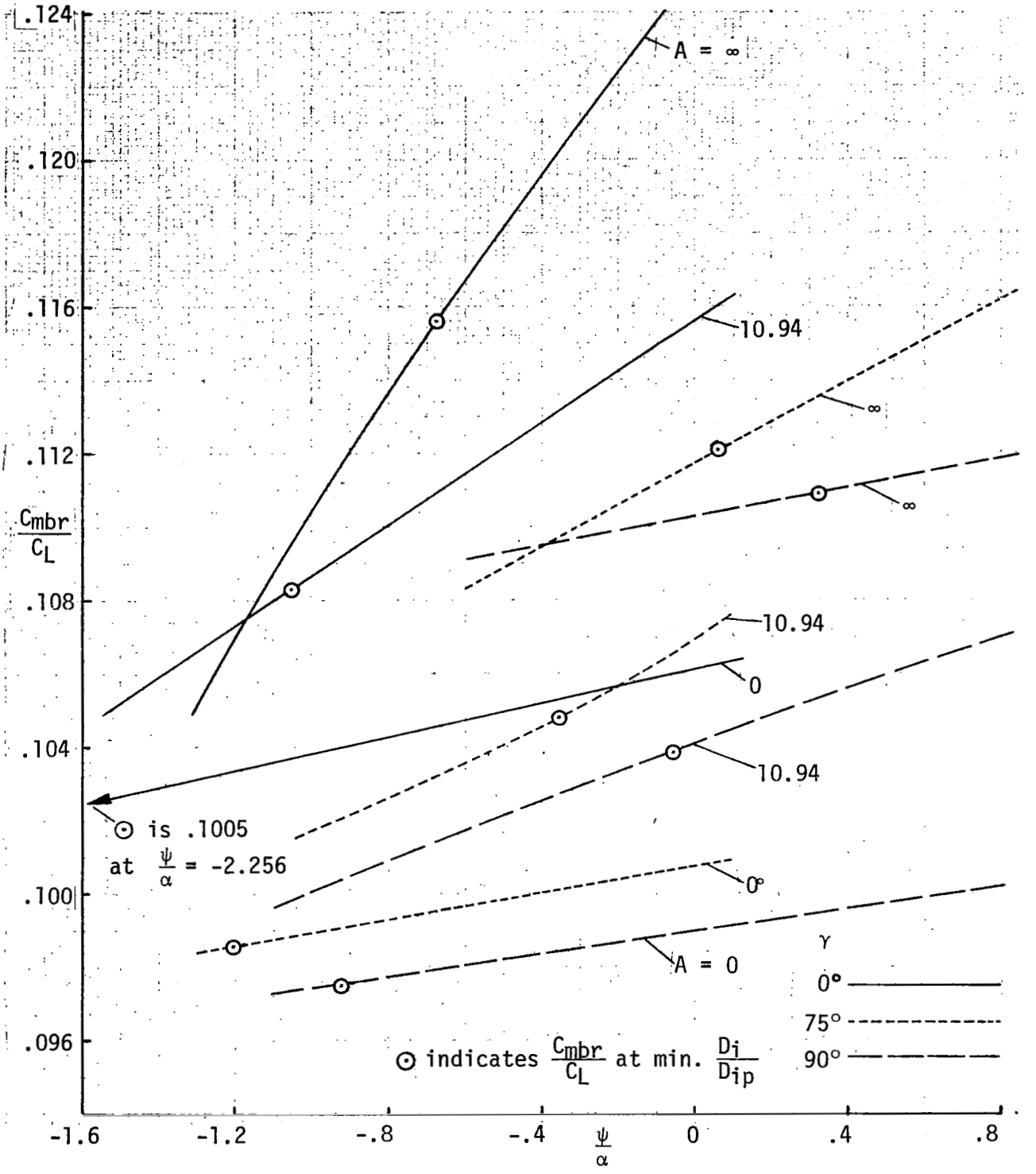

(b) Wing root bending moment coefficient of either wing.

Figure 2. - Continued

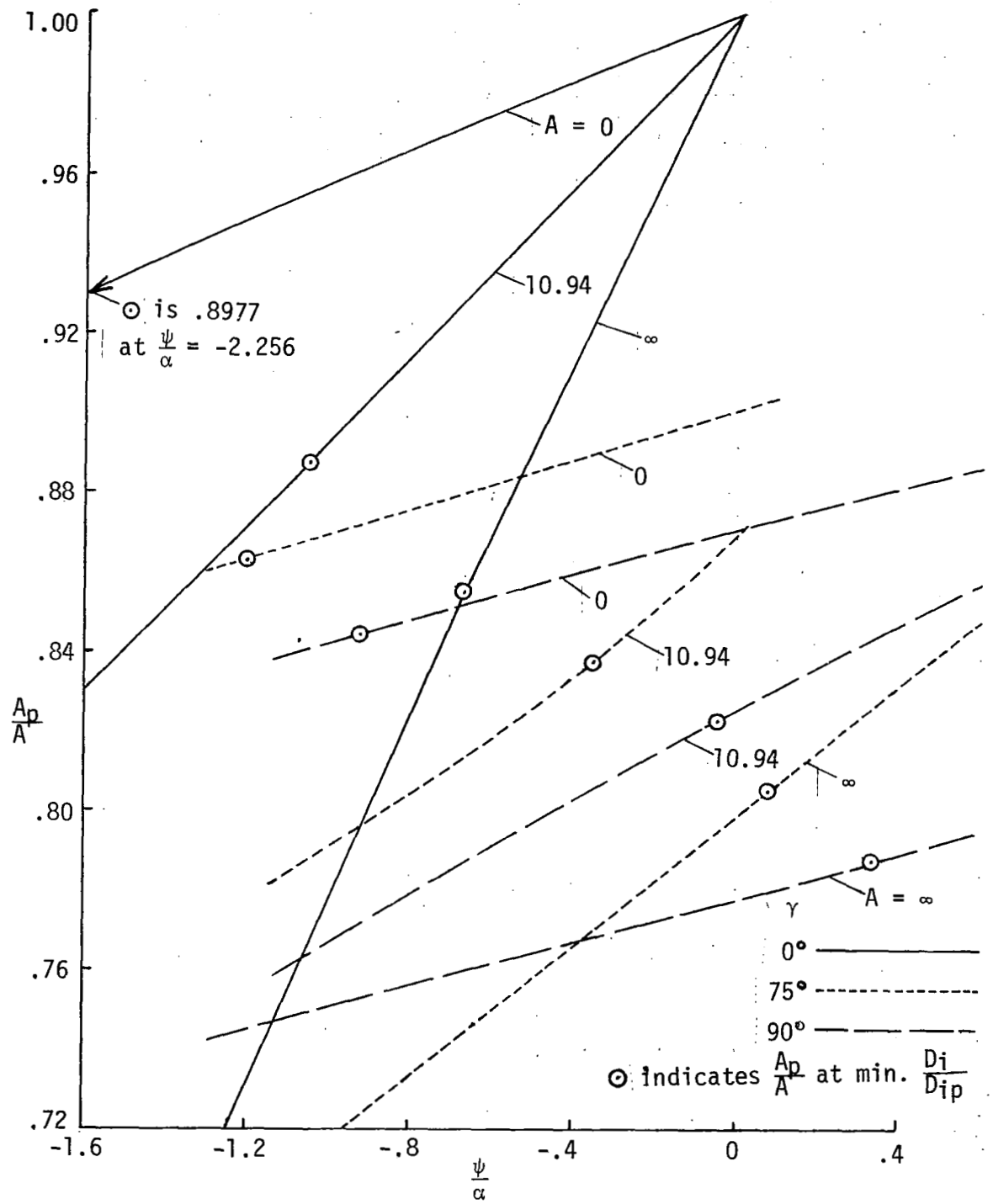

(c) Aspect ratio of planar wing.

Figure 2. - Concluded.

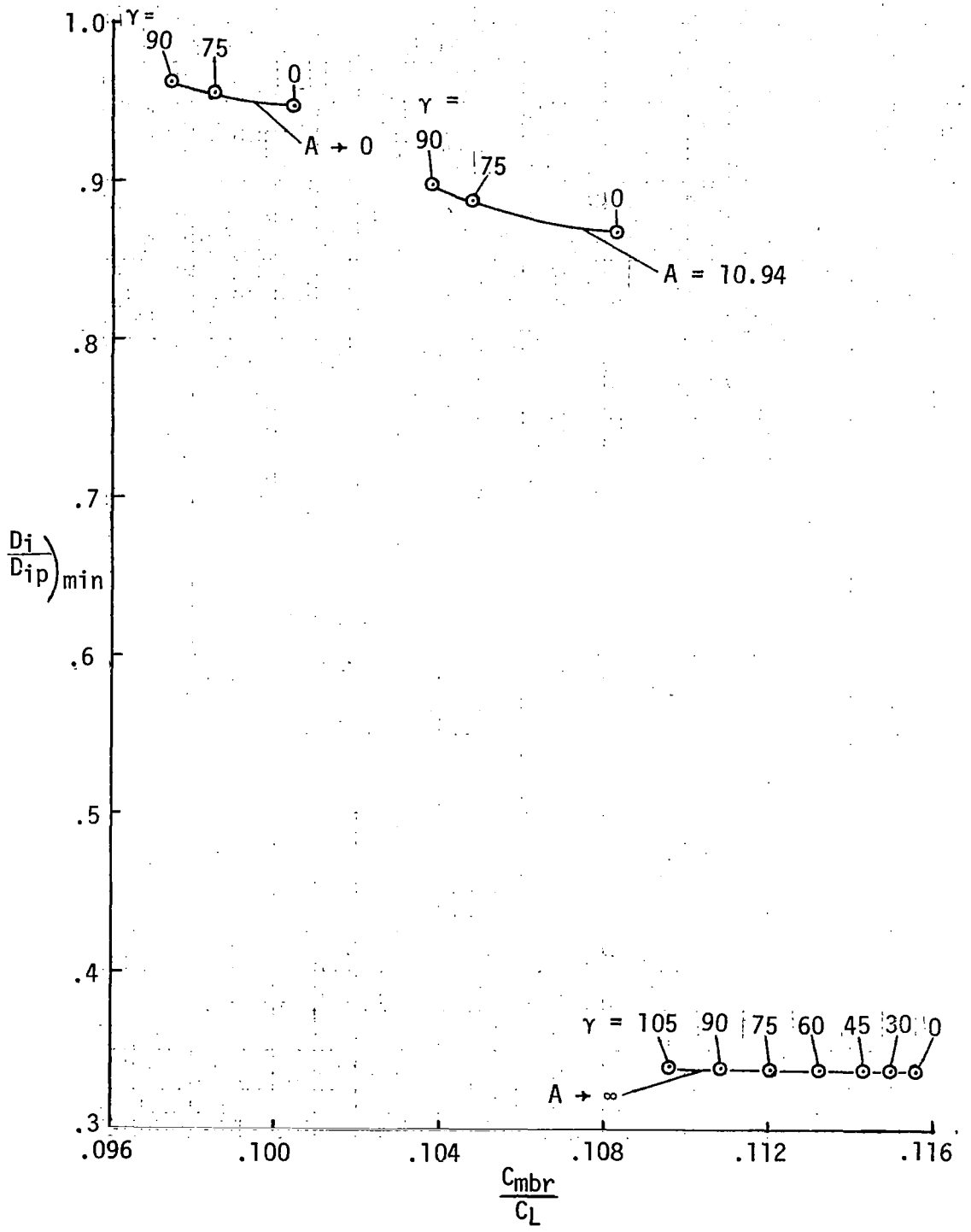

Figure 3. - Minimum induced drag as a function of wing root bending moment coefficient from data of figure 2. The angle γ, in degrees, is the winglet dihedral cant angle measured from the wing plane.

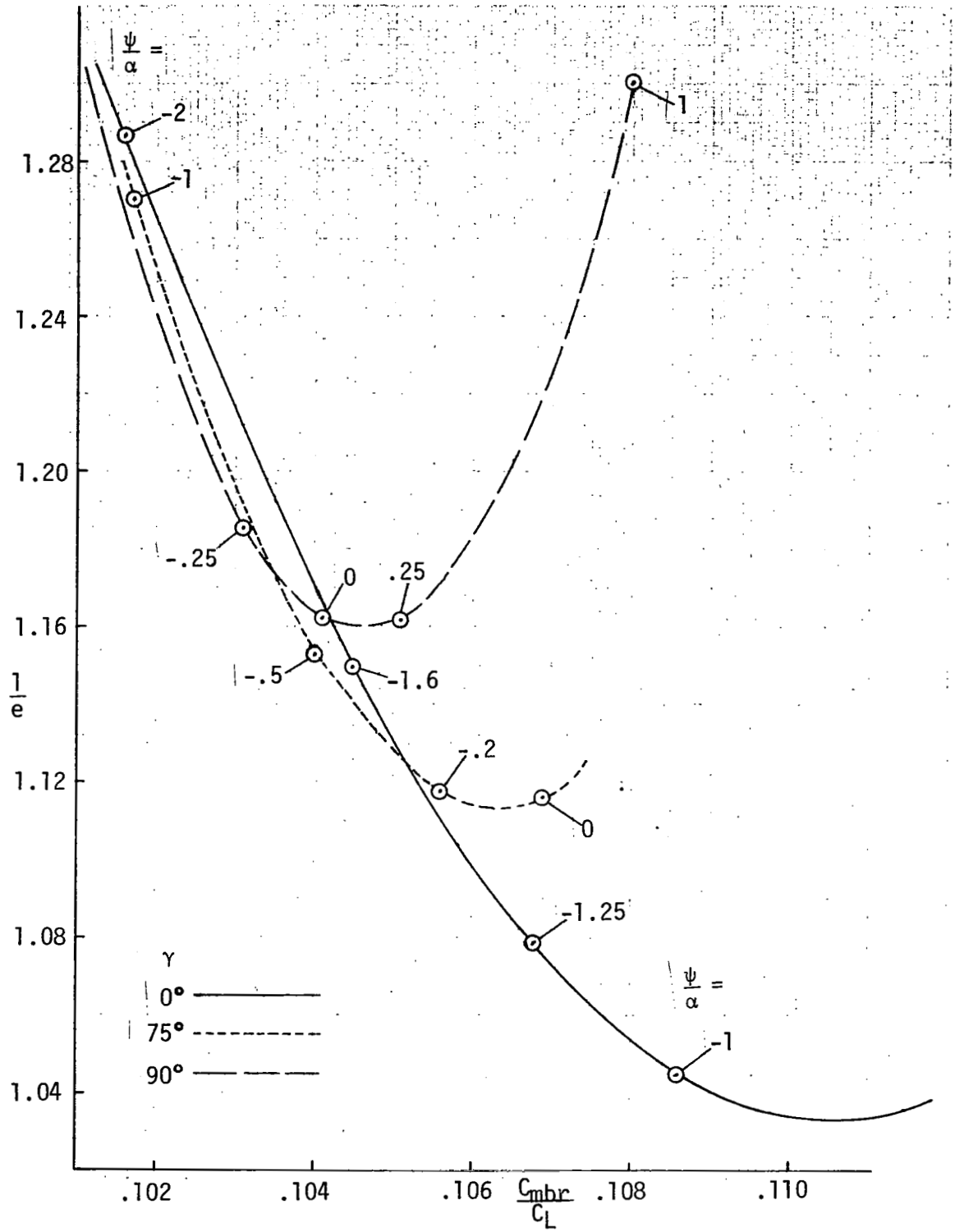

Figure 4. - Induced drag parameter $e^{-1} = \pi A C_{D_i}/C_L^2$ of A = 10.94 wing-winglet as a function of wing root bending moment coefficient, from data of Table V.